Incorporation of self-healing of UHPC in structural design approaches through healable crack width threshold and kinetics: The case study of H2020 project ReSHEALience database

Zhewen Huang [*], Estefania Cuenca, Liberato Ferrara

Department of Civil and Environmental Engineering, Politecnico di Milano, Italy

ARTICLE INFO

ABSTRACT

Ultra-high-performance concrete (UHPC) stands out as a crucial construction material, boasting outstanding mechanical properties and exceptional durability in its uncracked state. The distinctive strain-hardening tensile behavior of UHPC necessitates a consideration of material and structural durability in the cracked state, prompting a rethinking of structural concepts and design approaches. Consequently, various competing mechanisms, including material deterioration, self-sealing, and self-healing capabilities, require meticulous assessment. The autogenous nature of the self-healing capacity of the material, crafted with compositions tailored to specific mechanical properties, further underscores this evaluation. This study elucidates above concepts by compiling and analyzing an extensive database of crack closure data obtained and processed through image processing techniques. This research specifically delves into appraising the self-sealing capacity of UHPC under structural service conditions, encompassing challenges such as chloride and sulfate attacks. Additionally, it endeavors to distinguish the crack healing kinetics of diverse UHPC mix designs, calibrating them across varying crack widths (0–20, 20–50, 50–100, 100–300 μm) and diverse healing environments. These findings assume significance in establishing the "healable width threshold" and the "self-healing coefficients of the crack healing kinetics law" under "structural service conditions".

1. Introduction

The wide utilization of concrete in marine structures, transportation infrastructures, and chemical industry facilities exposes it to harsh environmental conditions (Al-Obaidi et al., 2021; Yao and Chu, 2023). Consequently, these structures undergo significant degradation and deterioration over time due to the presence of aggressive ions. Such degradation not only affects the service life of the structure but also leads to increased operating costs throughout its life cycle, as a result of the needed frequent repairs and modifications (Koch et al., 2005). To address these challenges, the utilization of High-Performance and Ultra-High-Performance Concrete in the aforesaid structural applications has been increasingly recommended and implemented (Al-Obaidi et al., 2022). It is worth remarking that, even in some aggressive exposure scenarios, concrete is designed to work in cracked state and the presence of small cracks (<100 or 200 μm wide according to the exposure conditions and design limit state) serves as a direct pathway for harmful substances to infiltrate and diffuse throughout the concrete matrix. In the case of UHPC, its signature tensile behavior helps in spreading the damage, otherwise localized into the aforesaid single crack, across a set of tightly spaced and thinly opened microcracks, whose formation and stable growth is visibly related to the strain hardening response. The formation and stable propagation of these micro-cracks, each of them only a few tens of microns wide, precedes the unstable localization of the same damage into a single major crack, which anyway represents the design target/threshold for serviceability limit states of UHPC structures. As a matter of fact, while surely implying tremendous benefits in terms of durability, this requires that also for UHPC the serviceability and durability have to be consistently addressed with reference to the specific characteristics of its cracked state.

In recent years, there has been a growing interest in materials and technologies that can autogenously and/or autonomously heal cracks, thereby enhancing the durability and service life of concrete structures at the same time balancing cost-effectiveness and high performance (Cappellesso et al., 2023; Hager et al., 2010; Nilimaa, 2023). Furthermore, there has been a recurring emphasis on integrating self-healing

---

concepts into durability-based code design approaches for structural applications of advanced cementitious materials to substantiate sustainable material development. This has to be done through an effective design-oriented quantification of the benefits in using these materials and achieve the sustainable development targets as a whole. Incorporating the effects of crack healing into a durability-based design framework may require the adoption of a "healable crack width" concept, which is defined as a function of material composition, expected exposure conditions, and structural service conditions, rather than the fixed "allowable crack width" concepts found in current design codes (Ferrara et al., 2016, 2018; Gupta et al., 2021) which are fixed mainly on the basis of a predefined exposure condition.

In this framework, it is important to provide an overview of existing self-repairing technologies for concrete, which consist of natural "autogenous" repair mechanisms and engineered "autonomous" repair techniques. The former relies on conventional components of the cementitious matrix, while the latter uses unconventional engineered additives to provide self-healing. The primary mechanisms underlying the autogenous healing of concrete within cracks encompass two essential processes: (1) carbonation of calcium hydroxide (CH), involving the reaction of CH in concrete with dissolved carbon dioxide from either air or water in exposed conditions, leading to the formation of calcium carbonate crystals within the cracks (Maddalena et al., 2021); and (2) the phenomenon of delayed hydration of unreacted cement particles. The latter process holds particular significance for UHPCs characterized by comparatively low initial water-binder ratios (Cuenca and Ferrara, 2017; Lo Monte et al., 2024; Sahmaran et al., 2013; Xi et al., 2023a).

Based on this healing technique, the possibility of crack healing ranges from a few tens of micrometers to 100 μm and up to even 300 μm, this healing also depends on the total time allowed for healing and its conditions (De Belie et al., 2018; Ferrara et al., 2017, p. 1; Sisomphon et al., 2012). The presence of water is essential to promote autogenous healing, so it is possible to stimulate or improve autogenous healing by adding superabsorbent polymers, hydrophilic crystalline admixtures and reinforcing hydration minerals to the concrete design, which not only accelerate the healing rate, but also allow the closure of cracks of larger widths (300–500 μm) (De Souza Oliveira et al., 2021; Qiu et al., 2016; Roig-Flores et al., 2015, 2016; Schröfl et al., 2022; Snoeck et al., 2020). The most widely investigated among the autonomous healing techniques are the addition of (encapsulated or granulated) microorganisms to cementitious materials, using the metabolic activity of the organisms to induce the precipitation of $CaCO_3$, a technique that allows for the closure of cracks of hundreds of μm to hundreds of mm (Wang et al., 2016) together with the use of encapsulated mineral and polymeric healing agents, which can, almost instantaneously, close cracks of several hundred μm, its effectiveness also depending on a balance between crack width, viscosity of the agent and capsule design (Ferrara et al., 2018; Kannikachalam et al., 2023; Van Tittelboom et al., 2011).In addition to the mixture design components mentioned above; however, the self-healing capacity of concrete cracks in structures is influenced by a multitude of factors, including initial crack shape and size, healing duration, hydraulic pressure gradient, temperature, humidity, loading, and exposure conditions and time (Muhammad et al., 2016; Van Tittelboom and De Belie, 2013; Wang et al., 2022; Xi et al., 2023a).

Based on the above characteristics of self-healing, and in order to incorporate them into durability-based structural design methods and codes, the "healable crack width" seems to be a relevant parameter (Gupta et al., 2021). In fact, crack width being a parameter with which structural designers are already familiar, when it comes to durability and serviceability limit states, and moreover it appears to be determinant for the evolution of its closure. On the one hand, the width directly influences the rate of crack closure, and on the other hand, in aggressive environments, it determines the entry of harmful ions, which enter the cracks by permeation, diffusion, and convection and counteract with the self-healing process through the cracks (Peng et al., 2019; Xu et al.,

Table 1
Mix-compositions of UHPC involved in experiment.

Constituents [kg/m³]	Labels for mixture design				
	CEM I	CEM I + CA	CEM I + CA + ANF	CEM I + CA + CNC	CEM I + CA + CNF
CEM I 52.5R	600	600	600	600	600
Slag	500	500	500	500	500
Water	200	200	200	200	200
Steel fibers Azichem Readymesh ®	120	120	120	120	120
Sand (0–2 mm)	982	982	982	982	982
Superplasticizer BASF Glenium ACE 300®	33	33	33	33	33
Crystalline admixtures Penetron Admix ®	–	4.8	4.8	4.8	4.8
Alumina nanofibers	–	–	1.5	–	–
Cellulose nanocrystals	–	–	–	0.9	–
Cellulose nanofibrils	–	–	–	–	0.9

2020). In recent years, the extensive experimental studies conducted on the self-healing properties of concrete has, as expectable, include the generation of cracks in a specific width range during the pre-cracking phase (Cappellesso et al., 2023; De Belie et al., 2018; Ferrara et al., 2018). However, the limited number of cracks distributed in a large number of different width intervals has hampered the study of the self-healing rate of cracks in specific width intervals. Additionally, variations in mixture designs among different research teams, including material types and mix proportions, as well as in crack creation and self-healing assessment methodologies have made it challenging to centrally compare and analyze collected crack data. Fortunately, the experimental work carried out in the Horizon 2020 ReSHEALience project has been able to provide a large amount of crack data, and these crack closure investigations were carried out entirely within the framework of a unified study, where the creation of pre-cracks mainly involved flexural and direct/indirect tensile tests of concrete beams, and where the crack geometry data were captured by the same image collection technique. These cracks were produced in different types of UHPC specimens, differing only in the presence of crystalline admixtures (CA) and nano-components, but the main concrete components remained highly consistent (Cuenca et al., 2021c; Cuenca et al., 2021d). The capacity of autogenous healing of UHPC subjected to different environments was investigated to achieve complete closure of the cracks, and the experimental campaigns covered curing loops including tap water, salt water, geothermal water, wet/dry cycles, and moist rooms.

This study is based on the database analysis of a five-year comprehensive experimental investigation as part of the ReSHEALience project, funded by the European Commission in the framework of the Horizon 2020 research and innovation program (GA760824), which, to the authors' knowledge is currently one of the largest public (www.uhdc.eu) homogeneous databases on the topic of crack self-healing in UHPCs, consisting of more than 700 cracks analyzed throughout a period of up to one year of exposure. The primary focus of this study is on the statistical analysis and visualization of a comprehensive crack image database, with the main objective of investigating the fully healable width threshold of cracks. This threshold has been quantified as a function of various influencing factors, such as mixture design, crack width dimensions, exposure time, and exposure environment. Another important aim of this study is to quantify the efficiency of autogenous healing by establishing the crack self-healing kinetic law. This has been achieved by adopting an exponential formula as a quantitative criterion for self-healing efficiency, thus calibrating the self-healing coefficients of cracks within different width ranges (0–20 μm, 20–50 μm, 50–100 μm, and 100–300 μm) across various environments. The above findings are of great significance in determining the "healable width thresholds" and " self-healing coefficients for the crack healing kinetic law " for "structural service conditions", which could potentially lead to the

Table 2
Composition of the geothermal water.

Constituent	Al	Ca	Fe	K	Mg	Na	S	Si	SO_4^{2-}	Cl
ppm	0.2	4	0.13	19.8	0.3	1243.2	1523.4	0.3	2678	441

Table 3
ICC Database construction from experimental work.

Reference	Mix design	Pre-crack tests	Exposure conditions	N° of specimens	N° of cracks
Xi et al. (2023b)	CEM I + CA	DEWS	Tap water, Salt water, Geothermal water	40	80
Davolio et al. (2023)	CEM I + CA CEM I + CA + ANF CEM I + CA + CNC	4PBt	Tap water Salt water Geothermal water	108	216
Cuenca et al. (2023)	CEM I + CA + CNF	4PBt	Geothermal water Moist room	12	51
Cuenca et al. (2021a)	CEM I + CA + ANF	4PBt, Splitting tests on disks	Geothermal water Moist room	23	119
Cuenca et al. (2021b)	CEM I + CA CEM I + CA + ANF CEM I + CA + CNC CEM I + CA + CNF	3PBt, Splitting tests on disks	Geothermal water Wet/dry cycles	86	86
Cuenca et al., (2021c)	CEM I CEM I + CA	4PBt, Splitting tests on disks	Tap water, Salt water	41	83
Lo Monte and Ferrara (2021)	CEM I + CA	4PBt	Wet/dry cycles	42	77

systematic incorporation of self-healing properties into durability-oriented design approaches for structural applications using advanced cementitious materials. By incorporating crack self-healing into the design phase, its benefits can be consistently exploited, rather than being seen as an elusive and often unquantifiable bonus.

2. Materials

Table 1 provides a comprehensive overview of the mix proportions employed in this study for the investigation of UHPC self-healing capacity. All the studies included in this analysis have utilized CEM I 52.5 R cement, which is a commonly chosen type in engineering and construction projects necessitating higher strength and early strength development, making it a fitting component for UHPC preparation. As customary in UHPC mix-designs, the total binder volume also incorporated a significant share of supplementary cementitious material, slag in this case, which was employed in equal volume percentage as cement. To achieve elevated matrix compactness and strength, sand with particle sizes ranging from 0 to 2 mm was selected as the aggregate, while maintaining a water-cement ratio of 0.33 (with a water-to-binder ratio of 0.18). Straight steel fibers measuring 20 mm in length and 0.22 mm in diameter were introduced at a volume fraction of 1.5% (Lo Monte and Ferrara, 2020), contributing to the cementitious composites' tensile hardening properties. The composition of the cement and slag, and the process of preparing the mixture are reported in detail in the previous investigations of the authors' research team (Cuenca et al., 2021a; Cuenca et al., 2021c).

In the design of the UHPC mixes, a careful balance between enhancing material performance and managing cost implications was sought, through incorporation of crystalline admixtures (CA) and nanomaterials (such as Alumina nanofibers, Cellulose nanocrystals, and Cellulose nanofibrils, investigated in this study) to suit specific service environments. In this research, a commercial crystalline admixture (Penetron Admix®) was used, which is easy to apply in concrete infrastructures and is the most reliable method to stimulate the self-healing properties of cementitious composites (Cuenca et al., 2018; Ferrara et al., 2014; Roig-Flores et al., 2015, 2016). The particle characteristics of CA resemble those of cement particles, featuring irregular shapes and sizes in the range of 1–20 μm (Ferrara et al., 2014). The mechanism by which CA stimulates the autogenous healing of concrete involves promoting the release of Ca^{2+} into the crack solution, elevating the pH of the pore solution, and accelerating the precipitation of $CaCO_3$, thus effectively sealing the cracks (De Souza Oliveira et al., 2021; Sisomphon et al., 2012; Van Tittelboom and De Belie, 2013). Furthermore, SEM and EDS analyses indicate that hydrated calcium aluminum sulfate minerals may also form, contributing to crack filling in addition to the generation of $CaCO_3$ through delayed hydration and carbonation reactions involving the cement and crystalline admixture.

The nanomaterials used in this study possess specific dimensional characteristics: Alumina nanofibers exhibit lengths ranging from 100 to 900 nm, diameters between 4 and 11 nm, and a surface area of 155 $m^2/$ g; Cellulose nanocrystals have an average diameter of 5 nm and lengths ranging from 50 to 500 nm; Cellulose nanofibrils vary in diameter from 5 to 20 nm, with lengths spanning from 50 to over 2000 nm. Adding the aforementioned nanomaterials to the cement, in an amount constituting less than 1% of the cement's weight, effectively ensures the development of the mechanical properties of the cement matrix, attributed to the nano-core effect of these nanomaterials (Han et al., 2017; Muzenski et al., 2019). The combination of crystalline admixtures and nano-components was strategically designed to improve and expedite the self-healing capacity of these composites, rendering them particularly suitable for aggressive environmental conditions (Cuenca et al., 2021a). In studies by the authors' research team at Politecnico di Milano, the synergistic effect of this mixture design on the one hand in controlling the crack width below few tens of microns threshold and in augmenting the self-healing capability of cementitious composites was explored and successfully confirmed, also in line with other previous studies (Anwar et al., 2020; Cuenca et al., 2021a, 2021b, 2022, 2023), as the presence of water serves as a favorable condition for the autogenous healing of concrete.

In order to incorporate elements of the structural service environment into the investigation, the campaign collected crack closure data from UHPCs in five different environments, detailed in Table 3, to investigate their healing properties. The specific environmental information is described below.

1. Tap water, taken from the public water network in Milan.
2. Salt water, i.e., an aqueous solution of sodium chloride at a concentration of 33 g/L.
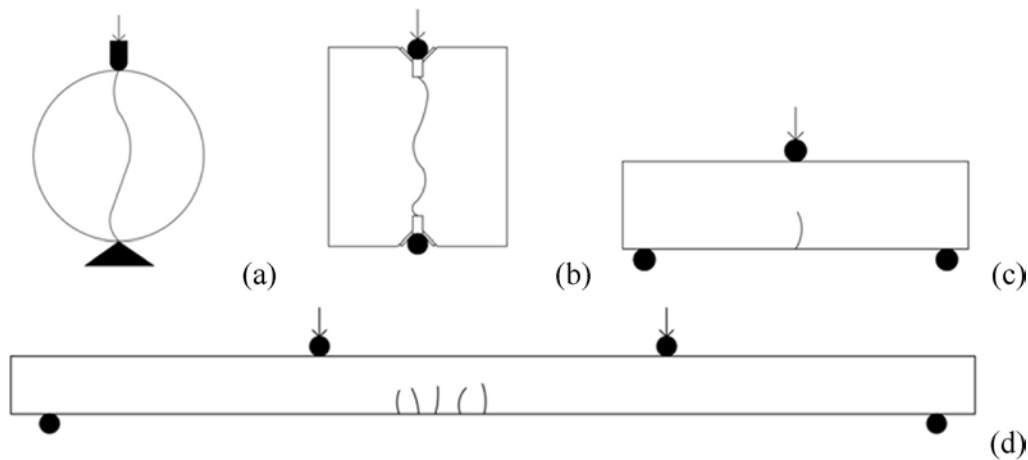
Fig. 1. Specimens used in the ReSHEALience experimental campaigns in pre-cracking: (a) Brazilian splitting cylinder; (b) DEWS specimen; (c) Thick beam; (d) Thin beam.
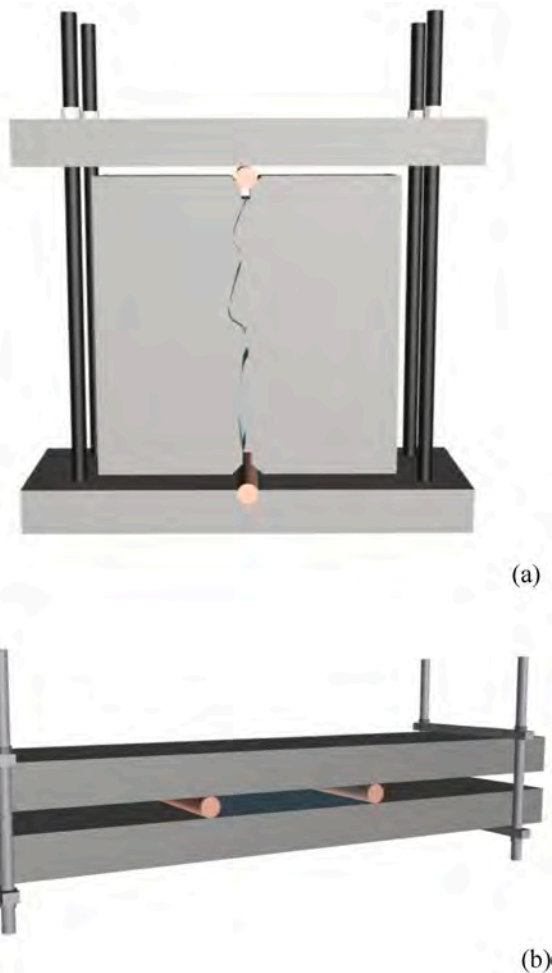

Fig. 2. Setups for sustained loading for: (a) DEWS specimen; (b) Thin beams.

3. Geothermal water, which was the most important exposure environment in the ReSHEALience project, with the water sourced from a geothermal power plant in Tuscany, Italy, supplied by Enel Green Power, a partner of the project. The chemical composition of the geothermal water is listed in Table 2.

4. Wet/dry cycles, in which the specimens were alternately immersed in geothermal water and in a climatic chamber with a relative humidity (RH) of 50% and a temperature of 20 °C.
5. Moist room, in which the temperature was maintained at 20 °C and the humidity at 95% RH.

3. Experimental program: tests and analysis methods

3.1. Pre-cracking test and setup of sustained loading

In this comprehensive database, a diverse collection of cracks was obtained from concrete test specimens featuring various shapes and sizes. The creation of cracks followed distinct approaches for different specimens, resulting in varying degrees of crack width and hence of crack healing, which, in turn, influenced the recovery of the mechanical and durability properties of the material. This study specifically emphasizes the analysis of the geometrical characteristics of the cracks under different exposure environments and encompasses data from multiple pre-crack tests to enhance the statistical robustness of the crack self-healing database (Fig. 1).

The characteristics of the concrete specimens and tests employed for crack healing characterization is outlined as follows.

- Splitting tests on disks (Ø100 mm × 80 mm, Ø100 mm × 60 mm – Fig. 1(a)) and Double Edge Wedge Splitting(DEWS) tests (100 × 100 × 25 mm3 – Fig. 1(b)) (Cuenca et al., 2021a; Cuenca et al., 2021c; Cuenca et al., 2023; Lo Monte and Ferrara, 2021; Xi et al., 2023b)
- 3-point-bending test(3PBt) on beams (40 × 160 × 40 mm3 – Fig. 1 (c)) (Cuenca et al., 2021b)
- 4-point-bending test(4PBt) on beams (100 × 500 × 30 mm3,100 × 500 × 100 mm3 – Fig. 1(d)) (Cuenca et al., 2021a; Cuenca et al., 2021c; Cuenca et al., 2023; Davolio et al., 2023; Lo Monte and Ferrara, 2021)

The experimental characterization of self-healing capabilities under sustained loading and through-crack stress states has been recognized as a critical and pressing research requirement. Addressing this need is imperative to establish a robust foundation for the integration of self-healing concepts and findings into predictive modelling and durability-based design methodologies (Ferrara et al., 2018). In this study, sustained loading was integrated into the analysis of healing capacity, Fig. 2 shows the two devices employed, each accommodating differently shaped specimen blocks. The specific load application process can be found in the work of the author's research group (Davolio et al., 2023; Xi et al., 2023b). The deflection hardening characteristics of
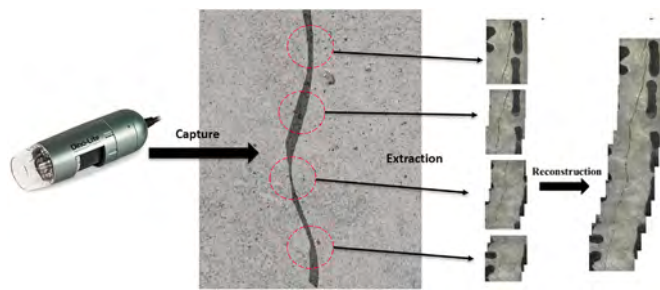
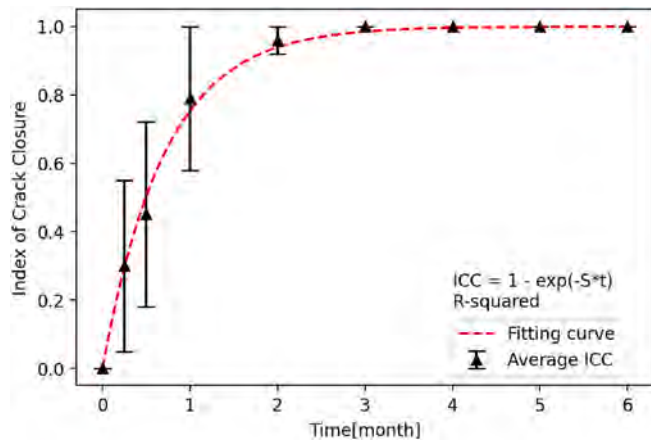**Fig. 3.** Schematic of image collection and processing of cracks.

Fig. 4. Fitting process for the kinetic coefficients of crack self-healing.

the materials guaranteed the ability to hold the load under the intended set-up, whose validation is anyway provided by Davolio et al. (2023).

3.2. Image collection technique captures cracks in healable progress

The assessment of crack self-healing primarily involves employing image collection techniques to capture the geometric characteristics of concrete cracks (Fig. 3). This process includes gathering crack information that arises after subjecting the specimen to a pre-cracking test, as

well as obtaining crack images following a specific healing time interval. Image processing techniques (utilizing Photoshop, 2020) were employed for measuring the length and area of the initial cracks, as detailed in the authors' prior publications (Cuenca et al., 2018), followed by the computation of initial crack width. Since crack closure is a dynamic process, the width and length of the cracks are variable in the healing process. Therefore, as a method to quantify the change in the area of progressively crack along the exposure time, meant as the healing progress, the Index of Crack Closure (ICC) has been employed, which has gained popularity in the field of self-healing concrete (Cappellesso et al., 2023; Ferrara et al., 2018). The involved formulas are as follows:

$$Initial\ Crack\ Width\ (ICW) = \frac{A_{pre-crack}}{L} \tag{1}$$

$$Index\ of\ Crack\ Closure\ (ICC) = \frac{A_{pre-crack} - A_{after\ healing}}{A_{pre-crack}} \tag{2}$$

where L represents the length of initial crack after pre-cracking; $A_{pre-crack}$ represents the initial area of the crack after the pre-cracking test; $A_{after\ healing}$ represents the crack area of the same specimen after exposure to different curing environments.

The ICC serves as a crucial metric for assessing the healing performance of concrete and it has been further correlated with the recovery of strength and stiffness in the concrete. The robust correlation observed between water permeability recovery and crack closure validates the measurement reliability, as supported by the outcomes of water flow tests detailed in the authors' prior publications (Cuenca et al., 2021a, 2023). Therefore, the ICC has constituted the fundamental basis for establishing the database and conducting in-depth analyses in this research. Furthermore, the inclusion of a sufficient number of cracks under various multivariate conditions ensures the feasibility and rationality of the database creation and analysis.

It is worth reminding once more that a total of 712 cracks were subjected to pre-cracking tests for which geometric information was collected, all from the papers mentioned in Table 3 used to construct this ICC database. The papers were all published in the framework of ReSHEALience H2020 project. The pre-cracking test methods, exposure environments and mix designs are also well demonstrated in detail.
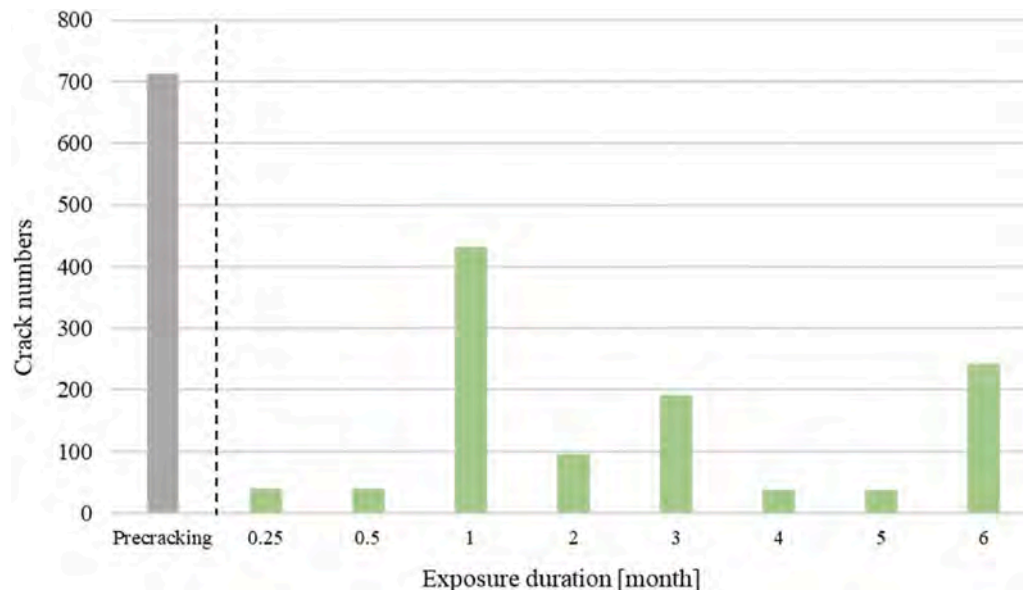

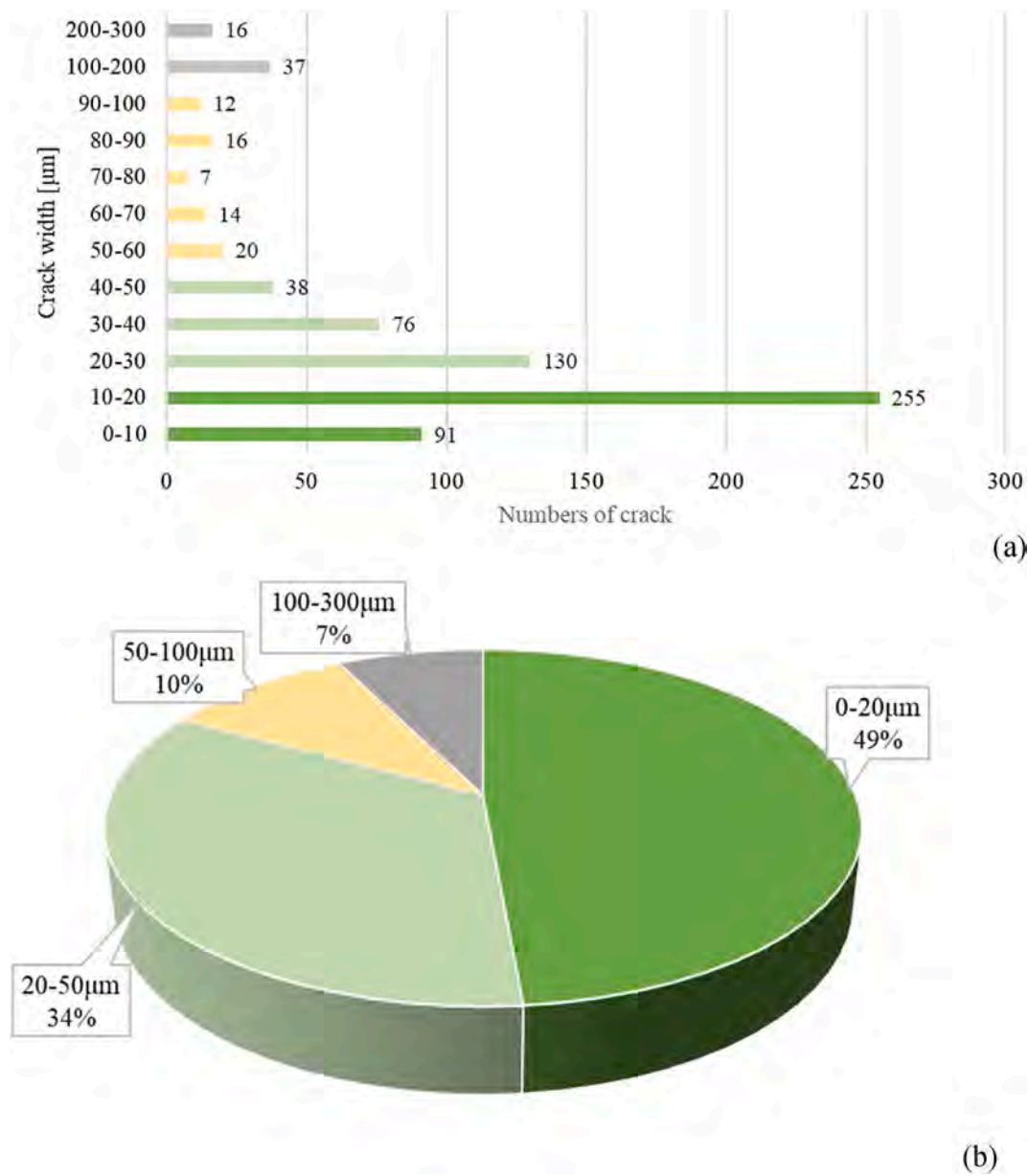**Fig. 5.** Number of cracks per duration of the exposure period.

Fig. 6. Statistics of cracks in different width ranges: (a) number (b) percentage.

3.3. Calibration method for crack kinetic self-healing coefficient

In order to comprehensively calibrate the kinetic law governing crack self-healing (see Fig. 4), this study employs a commonly used exponential decay formula (Istratov and Vyvenko, 1999) that accounts for fundamental healing phenomena: (1) the ICC is 0 at the initial moment; (2) rapid closure of cracks within the first month; and (3) gradual complete closure of cracks (ICC = 1) over extended healing time in an aqueous environment. The formulas utilized are as follows:

$$ICC_{average} = 1 - e^{-S \bullet t} \tag{3}$$

where t is the curing time for specimens exposure in different environments; S is self-healing coefficient for cracks under water environments which indicates the rate of crack closure; $ICC_{average}$ represents the average value of crack closures that have undergone a specific curing time.

By incorporating the exposure environment, crack width, and mixture design, which are the key factors influencing the rate of

autogenous healing of concrete, this calibration process enables the accurate establishment of the healing rate-time relationship for specific conditions, offering invaluable insights into the mechanisms of crack healing. The derived calibration equations serve as a fundamental foundation for subsequent research and modelling of crack healing behavior, thereby advancing our comprehension of the self-healing capabilities of the investigated materials.

4. Results and discussion

4.1. Crack number in database

4.1.1. Number of cracks collected per exposure duration

After a distinct exposure period for each environment, the geometric properties of the cracks were retrieved once more. The establishment of the database involved several pilot studies within the ReSHEALience project, focusing on exploring the healing properties of UHPC. Slight variations in the test protocols resulted in different numbers of cracks being collected for each exposure duration. Some cracks were scheduled
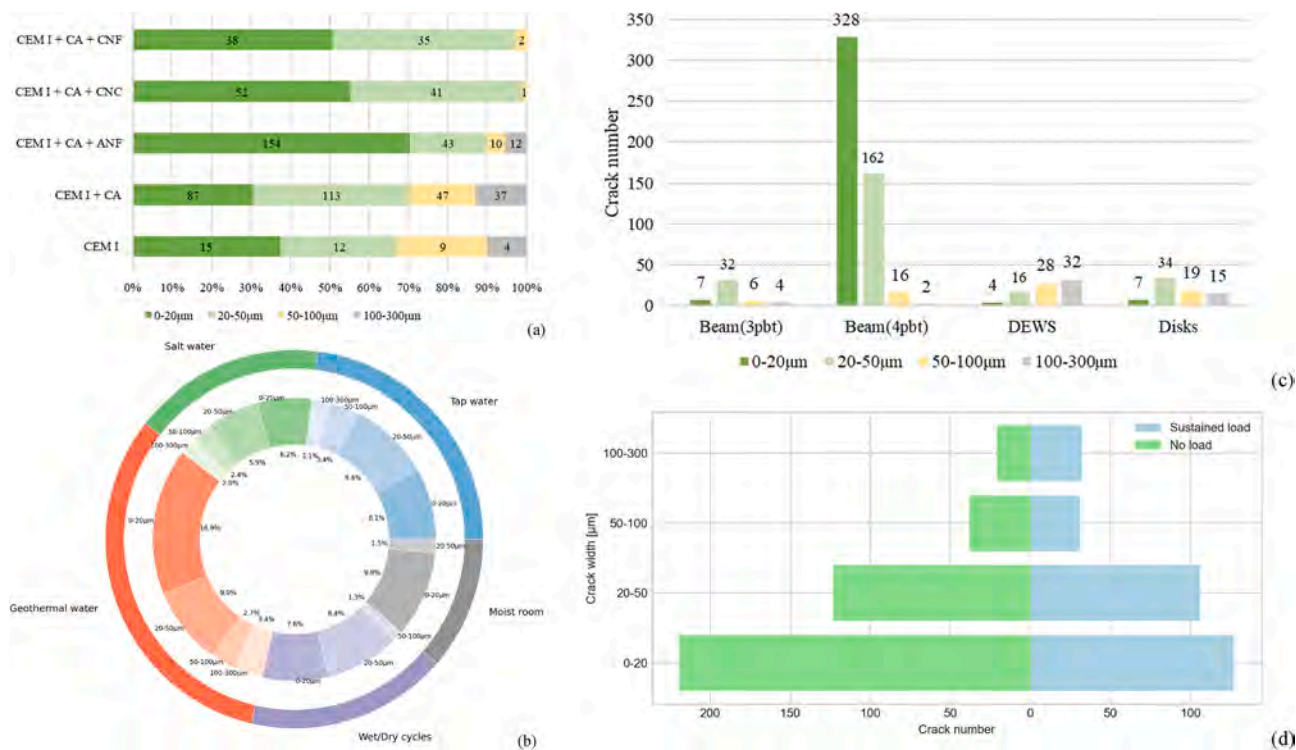
Fig. 7. Dualistic taxonomy of crack number with width as the primary element and secondary element: (a) Mix design; (b) Exposure environment; (c) Experimental method for pre-cracking; (d) Sustained load.

for exposure periods shorter than 6 months, while others underwent consecutive exposure durations to track healing progress, with data collection conducted for each specific duration (Fig. 5). Additionally, certain cracks completed healing within a specific brief period. The dataset exhibits certain discrete points or areas of ambiguity in subsequent analyses; however, these do not undermine the assessment of crack healing tendencies under specific conditions. It is worth remarking that the largest number of cracks which were monitored after 1, 3 and 6 months of healing time was able to provide enough data for the calibration of the crack self-healing coefficients. On the basis of the reliability of the analysis, the data was extensively utilized for broadest applicability.

It is worth here remarking that some of the studies of the database herein analyzed also included cracks surveyed up to one year of exposure in different conditions; anyway for all of them the complete sealing (ICC = 1) was achieved already before the aforesaid deadline, which henceforth results into them not being any longer significant in the calibration of the self-healing kinetics law.

4.1.2. Crack distribution by width range

Fig. 6(a) shows the distribution of crack numbers across various width ranges, encompassing a total of 712 cracks of varied sizes included in the study's database. Following the pre-cracking tests, the concrete specimens were subjected to specific environmental conditions. Previous research has consistently (De Belie et al., 2018; Xi et al., 2023a; Xue et al., 2023) demonstrated that the autogenous healing mechanism of concrete is predominantly influenced by factors such as crack width, exposure environment, and duration. Through a data-driven model employing artificial intelligence and machine learning, Xi et al. (2023b) identified exposure time and crack width as critical parameters in three different water environments for predicting self-healing performance. To conduct a thorough analysis and quantitative assessment of the effect of crack width on the self-healing of UHPC, the number of cracks was meticulously tallied and categorized based on the respective crack width intervals, as illustrated in Fig. 6(b). Specifically, the crack widths are

classified into four distinct healable width ranges: 0–20 μm, 20–50 μm, 50–100 μm and 100–300 μm. Subsequently, comprehensive analysis was conducted to examine the rate of crack closure and the effectiveness of healing in specific exposure environments.

4.1.3. Dualistic taxonomy of crack number

Fig. 7 shows the dualistic taxonomy employed for further analyzing and categorizing the number of cracks in this study. The taxonomy encompasses the crack width as the primary element and includes numerous factors such as mixture design, exposure environment, precracking test methods, and the presence of sustained load on the test specimen as secondary elements that influence crack healing.

Crystalline admixtures (CA) significantly contribute to stimulating the autogenous healing of cracks, and this study extensively accounts for the number of cracks containing CA. The mechanism of operation of the synergistic effect of nano-constituents and CA on the self-healing of concrete has been revealed by (Cuenca et al., 2021b). In the context of structural design, nanomaterials have demonstrated a pivotal contribution in addressing diverse and challenging environmental conditions by expanding the range of crack-healable widths and enhancing the rate of healing for small cracks (Al-Obaidi et al., 2020; Cuenca et al., 2022). Therefore, alumina nanofibers were used as the main material in the concrete design of ReSHEALience's UHPC, which is presented in Fig. 7 (a). It is important to highlight that geothermal water was selected as the extreme aggressive environment for concrete exposure within the scope of this project. In Fig. 7(b), approximately one-third of the total number of cracks in the database deal with exposure to geothermal water, while the remaining four exposed environments accounted for a comparable percentage of the overall crack count.

The cracks were primarily induced through the aforementioned four pre-cracking tests, and image capture techniques were employed on the four distinct concrete specimens with varying geometries, as depicted in Fig. 7(c). During the 4-point bending test, multiple cracks were often produced on a single specimen. Although the concrete specimens subjected to different pre-cracking tests exhibited variations in the loss of

Table 4
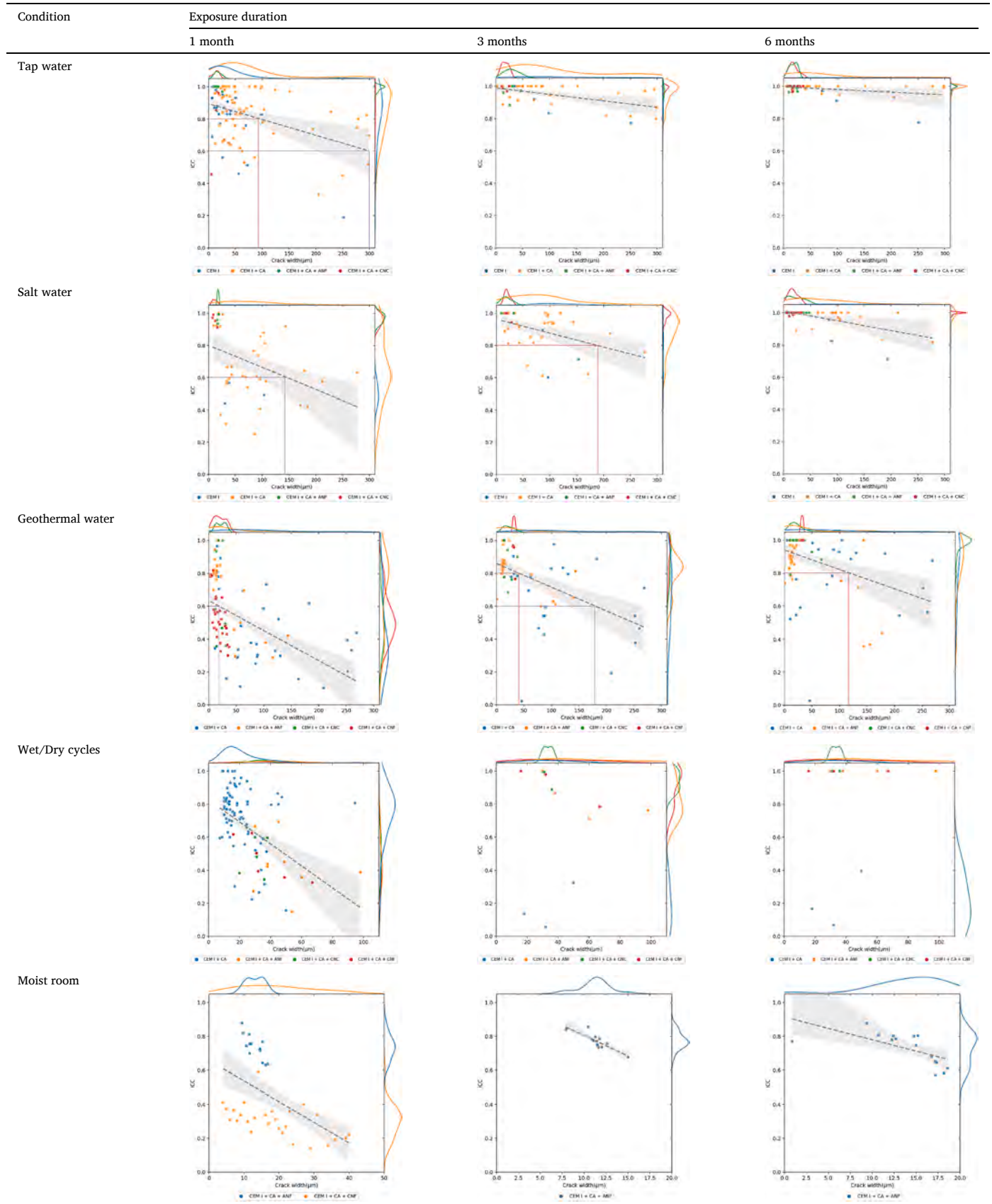ICC vs. Crack width in different specific exposure conditions.

Condition	Exposure duration		
	1 month	3 months	6 months
Tap water			
Salt water			
Geothermal water			
Wet/Dry cycles			
Moist room			

Table 5

Approximation of threshold crack widths corresponding to ICC reaches 0.8 and 0.6 from linear regression functions.

Environment	Exposure duration					
	1 month		3 months		6 months	
	ICC = 0.8	ICC = 0.6	ICC = 0.8	ICC = 0.6	ICC = 0.8	ICC = 0.6
Tap water	100 μm	300 μm	>300 μm	>300 μm	>300 μm	>300 μm
Salt water	≤20 μm	150 μm	200 μm	>300 μm	>300 μm	>300 μm
Geothermal water	≤20 μm	20 μm	50 μm	180 μm	120 μm	≥300 μm

mechanical properties, no significant differences were observed in the physical closure of the cracks. The effect of the presence of sustained loads on the healing effect of cracks is worth being discussed in a multidimensional way, especially on the mechanical properties of concrete (Mirshahmohammad et al., 2022; Zhang et al., 2020). Crack closure as an important reference factor for concrete healing and the presence of sustained loads on its recovery effect cannot be ignored, Fig. 7(d) shows the number of cracks present in each width range in this database.

4.2. Crack sealing capacity as a function of the experimental variables identifying the database

After having defined the taxonomy of the crack database, the evolution of the ICC, has been analyze as a function of mixture design, exposure environment, and applied load also to assess the impact of the aforesaid parameters on the autogenous healing mechanism of concrete and as a mean to establish thresholds for the width of healable cracks, as a function of the experimental variables as above.

4.2.1. Healing Promotor: CA and nano constituents

Table 4 presents a comprehensive summary of the relationship between the ICC and crack width. It encompasses various concrete specimens featuring distinct healing promoters and subjected to different exposure conditions. Two pivotal experimental variables, the exposure environment and exposure duration, significantly influence the crack closure process. To find the potential positive effect of CA with nanomaterials on the self-sealing and self-healing ability of the specimens. Accordingly, the ICC values have been plotted for diverse mixture designs under specific exposure environments and durations. It is clearly found that especially in curing environments of tap water and salt water, the presence of CA exhibited limited discernible effects on crack closure when the crack width was below 50 μm. This observation can be attributed to the inherent ability of small-sized cracks to naturally undergo self-generated healing, especially in a material like UHPC featuring high binder content and low water-binder ratio (Lo Monte et al., 2024). Conversely, as the crack width expanded, the stimulating effect of CA on the healing response became increasingly evident, enhancing the self-sealing attributes, particularly at wider crack widths. In the case of tap water, cracks exceeding 200 μm in width exhibited ICC values exceeding 0.6 for the majority of cases after one month of exposure. Similarly, in salt water, the amplified effect of CA-stimulated self-generated healing became significantly pronounced after three months of exposure. A substantial portion of cracks containing CA displayed ICC values of 0.8 or higher, while the relative healing capacity of the concrete without it was slightly poorer.

The incorporation of meticulously tailored nanoscale constituents into the CA-based mixture within UHPC serves the primary purpose of bolstering the long-term durability of concrete when exposed to extremely aggressive environmental conditions. Remarkably, this material customization approach yields outstanding results in terms of crack healing performance. In both salt water and tap water, cracks narrower than 50 μm exhibit high healing efficacy, with ICC surpassing 0.8, and in certain cases, even reaching 0.9, after just one month of exposure. In the presence of UHPC with ANF in geothermal water, the

closure of cracks narrower than 50 μm was notably expedited, with the ICC converging around 0.8 within a month. While the enhancement of concrete healing facilitated by CNF in this environment appears slightly inferior to ANF initially, after an extended period of immersion, CNF and CNC had a higher completion of complete crack closure. When the width is larger than 50 μm, the experimental works specifically focuses on cracks within concrete specimens featuring ANF in geothermal water, as no distinct healing patterns emerge for other scenarios.

In the wet-dry cycle, an intriguing phenomenon unfolded where cracks narrower than 20 μm (comprising solely UHPC with CA) exhibited substantial healing within a month's duration. Their ICC distribution ranged from 0.6 to 1, possessing a remarkably high quality of self-healing. This underscores the significance of crack width as a pivotal parameter in evaluating the concrete's closure capability. The effect of individual nanomaterials on crack closure could not be clearly determined for wider cracks. Nevertheless, as the exposure period extends beyond three months, the ICC values for concrete containing nanomaterials exceed 0.8, highlighting their sustained healing efficacy. Notably, during the initial stages of healing in the moist room, the impact of ANF on crack healing performance is conspicuously superior to that of CNF, aligning with the observed trend in the geothermal water environment.

Table 5 supplies a summary of the threshold crack widths estimated through linear regression analysis for ICC values up to 0.8 and 0.6, excluding consideration of the mixture design.

4.2.2. Exposure environments

The development of healing products within cracks is determined by factors such as the presence of liquid water, ambient temperature, humidity, and chemical ion composition of the environment. Fig. 8 presents the distribution of Index of crack closure for cracks exposed to various environments across a range of different widths. It also illustrates the distribution of ICC for cracks after self-healing following specific exposure durations (1 month, 3 months, and 6 months). These analyses provide insights into the effectiveness of crack healing and its variation across different exposure environments.

Fig. 8(a) illustrates the distribution of ICC within various width ranges for cracks exposed to different environments after one month of self-healing. Cracks immersed in tap water have the largest median values in their respective width ranges, and it is interesting to note that the violin plots for widths of 0–20 μm show wider upper widths and narrower lower widths. These visual characteristics indicate that most of the cracks achieve an ICC in the range of 0.8–1, and as the crack widths increase, the distribution of ICC values becomes more dispersed, albeit with a significant proportion still exhibiting high healing ability. This confirms the notable level of self-healing capacity for tap water immersion.

It is essential to investigate the influence of crack width on the ICC in different exposure environments, as it not only impacts the rate of self-healing but also affects the infiltration of harmful substances into the cement matrix (Peng et al., 2019; Reinhardt and Jooss, 2003). As the crack width increases, the efficacy of crack sealing diminishes. In the case of cracks immersed in salt water, after one month, those with widths of 0–20 μm exhibit an ICC of 0.9 or higher, while the median value for cracks wider than 20 μm is approximately 0.6. This trend
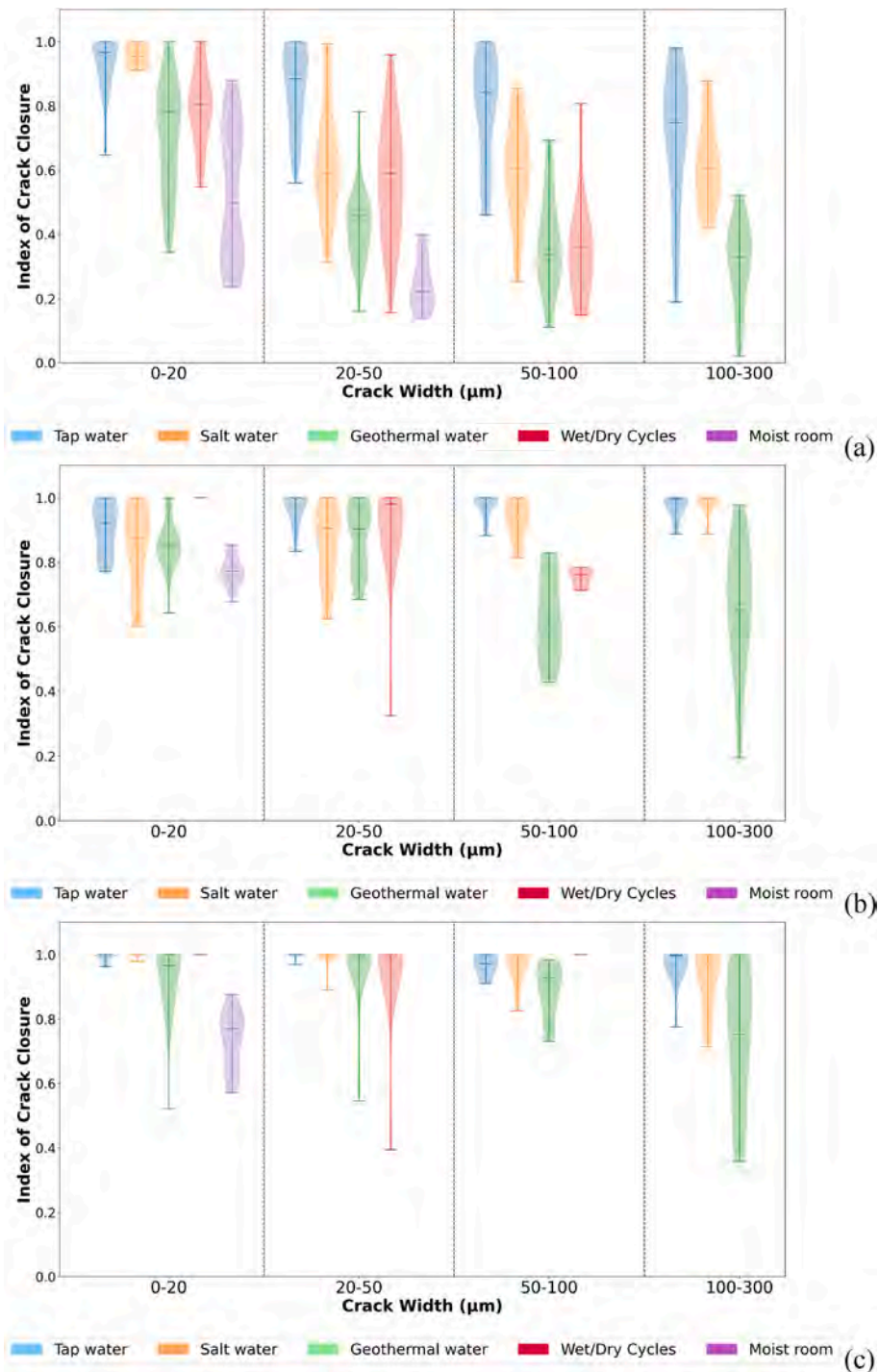
Fig. 8. Index of crack closure in different exposure conditions after (a) 1 month; (b) 3 months; (c) 6 months.

differs significantly from that observed in cracks exposed to other aqueous environments. Hence, a width threshold of around (and slightly greater than) 20 μm exists for cracks exposed to salt water, serving as a healable width threshold. Beyond this threshold, up to 300 μm, the healing ability of concrete immersed in salt water at this concentration remains relatively consistent.

Cracks exposed to geothermal water also exhibit a complete sealing width threshold below 20 μm. However, the prolonged presence of high concentrations of sulfate and chloride ions hinders the formation of the healing product $CaCO_3$ (Qian et al., 2019), thus affecting the rate of self-healing. This observation is further supported by the comparison of crack healing effectiveness between geothermal water and wet/dry

Table 6
Maximum width range for found crack fully healed under specific healing conditions.

Exposure environment	Exposure duration		
	1 month	3 months	6 months
Tap water	50–100 μm	100–300 μm	100–300 μm
Salt water	20–50 μm	100–300 μm	100–300 μm
Geothermal water	0–20 μm	20–50 μm	100–300 μm
Wet/Dry cycles	0–20 μm	20–50 μm	50–100 μm
Moist room	–	–	–
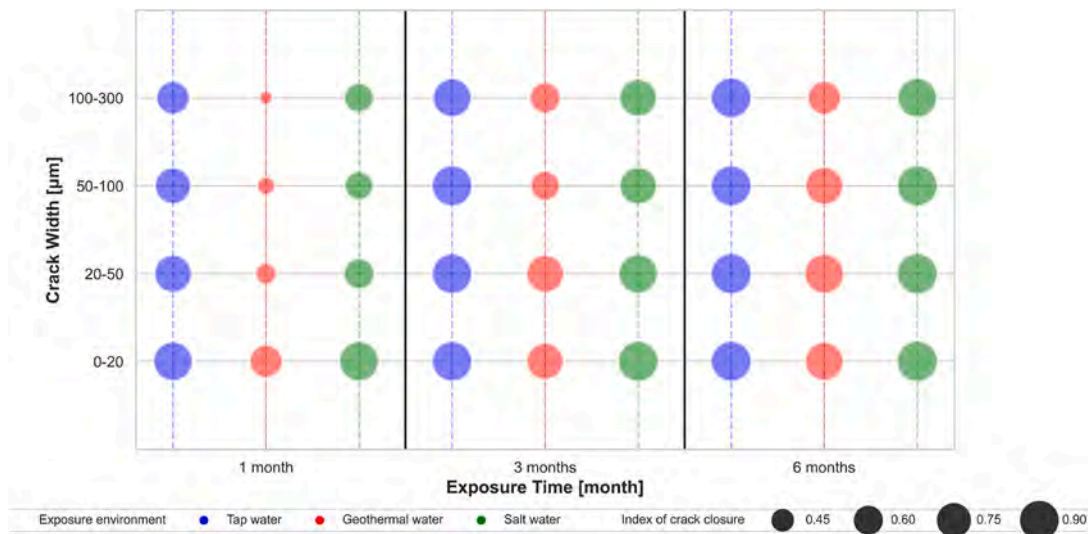
Fig. 9. The average ICC in each width range after the specified exposure duration for the three water environments.

cycles, where cracks in geothermal water display slightly lower healing ability across all width ranges. Additionally, cracks exposed to a moist room environment exhibit highly scattered and lower ICC values, even within the smallest crack width range, with median values hovering around 0.5. The level of crack healing in this environment is much lower, particularly in the 20–50 µm crack width range.

As depicted in Fig. 5, the number of collected cracks varied across different exposure durations, resulting in a small number of violin plots with decreasing median and minimal values as healing time increased. Nevertheless, crack healing exhibits a positive trend with longer exposure periods, as evident from the visual changes in the graphs. Each violin plot within the width range displays a widening upper part and a narrowing lower part as exposure time changes (Fig. 8). The width boundaries of fully healable cracks gradually expand with prolonged exposure time in the four environments: tap water, salt water, geothermal water, and wet-dry cycles. Table 6 summarizes the maximum range of fully healed crack widths identified for each exposure environment. However, for moist rooms, a specific range of fully healed crack widths could not be determined in this research study. Fig. 8(c) illustrates that even after 6 months of extended exposure, the ICC of the cracks remains concentrated around 0.8, indicating limited healing capability in this environment.

The inclusion of microfibers in the concrete formulation restricted the crack widths to a range that could be effectively healed. Specifically, in the case of wet/dry cycling, fully healed crack widths ranged from 30 to 50 µm, which falls below the non-healing criterion of 150 µm (Snoeck et al., 2014; Yang et al., 2009). While the number of cracks in the 0–20 µm range was limited in this environment after a 3-month curing period, the few cracks collected demonstrated complete closure (Fig. 8(b)). This trend persisted even after 6 months of healing time, as illustrated in Fig. 8(c).

Fig. 9 shows a comparative analysis of the average ICC in each width range after the specified exposure duration for the three water environments. Tap water consistently demonstrates the highest level of crack self-healing, as supported by numerous studies. Notably, after a one-month healing period, the influence of crack width on the healing performance of cracks exposed to geothermal water becomes evident. The subsequent sections provide a quantitative assessment of the impact of exposure duration on the effectiveness of crack healing. Additionally, longer exposure periods are favorable for achieving crack closure.

4.2.3. Sustained load

In order to provide an estimate of the crack sealing capability in

realistic structural service scenarios, including the effects of sustained load and through crack sustained stress in the analysis is of the utmost importance since this replicates the condition the material will experience in any structure when in service. In fact, a positive effect of the sustained load was detected on the healing capacity of the cracks, which were divided into four width range scales in the three aqueous environments: tap water, salt water and geothermal water, as it can clearly be seen in Fig. 10. The height of the bar represents the mean value of the ICC, and this data label is placed at the top of the graph. Notably, the difference in mean of ICC within the 50–100 µm range reached approximately 0.2. For cracks initially falling within the 20–50 µm range and exposed to geothermal water, the presence of applied load approximately doubled the effectiveness of crack closure compared to conditions without load. As the exposure duration extended, the cracks in each specific condition displayed robust closure, aligning with the principles of kinetic law governing crack self-healing.

Large cracks of 100–300 µm are less affected by loading. Although the enhancement of the crack healing effect by sustained loading is still observable (Fig. 10 (a, c)), the migration of large amounts of sulfate and chloride ions into the cracks is accelerated as the crack width scale tends to larger values, which in turn slows down the onset of the self-healing reaction of filling the cracks with calcium carbonate crystals (Liu et al., 2020). The variability of the ICC decreases markedly in larger cracks.

According to the above analysis, the presence of sustained loading is conducive to the occurrence and process of autogenous healing of UHPC. This is attributed to the phenomenon of creep in concrete structures (Liu et al., 2024), leading to continuous microcrack generation within the concrete matrix under prolonged loading. Consequently, substantial water imbalances occur, causing water concentration gradients and pressure gradients. These gradients drive water vapor from the capillaries around microcracks towards them (Fick's Law) and liquid water movement (Darcy's Law) (Rossi et al., 2013). The microcracks created serve as pathways for liquid water, accelerating the hydration kinetics of both hydrated and non-hydrated cement particles. This phenomenon contributes to the self-healing of microcracks.

4.2.4. Calibration of crack self-healing kinetic models

Calibrating the kinetic models for crack closure involves determining the self-healing kinetic coefficient (S) in Equation (2), which represents the rate of crack self-healing. The value of R^2 serves as one of the factors used to assess the quality of the fitting. Table 7 presents the self-healing kinetic coefficient (S) alongside the corresponding R-squared values obtained by fitting the function to different exposed water
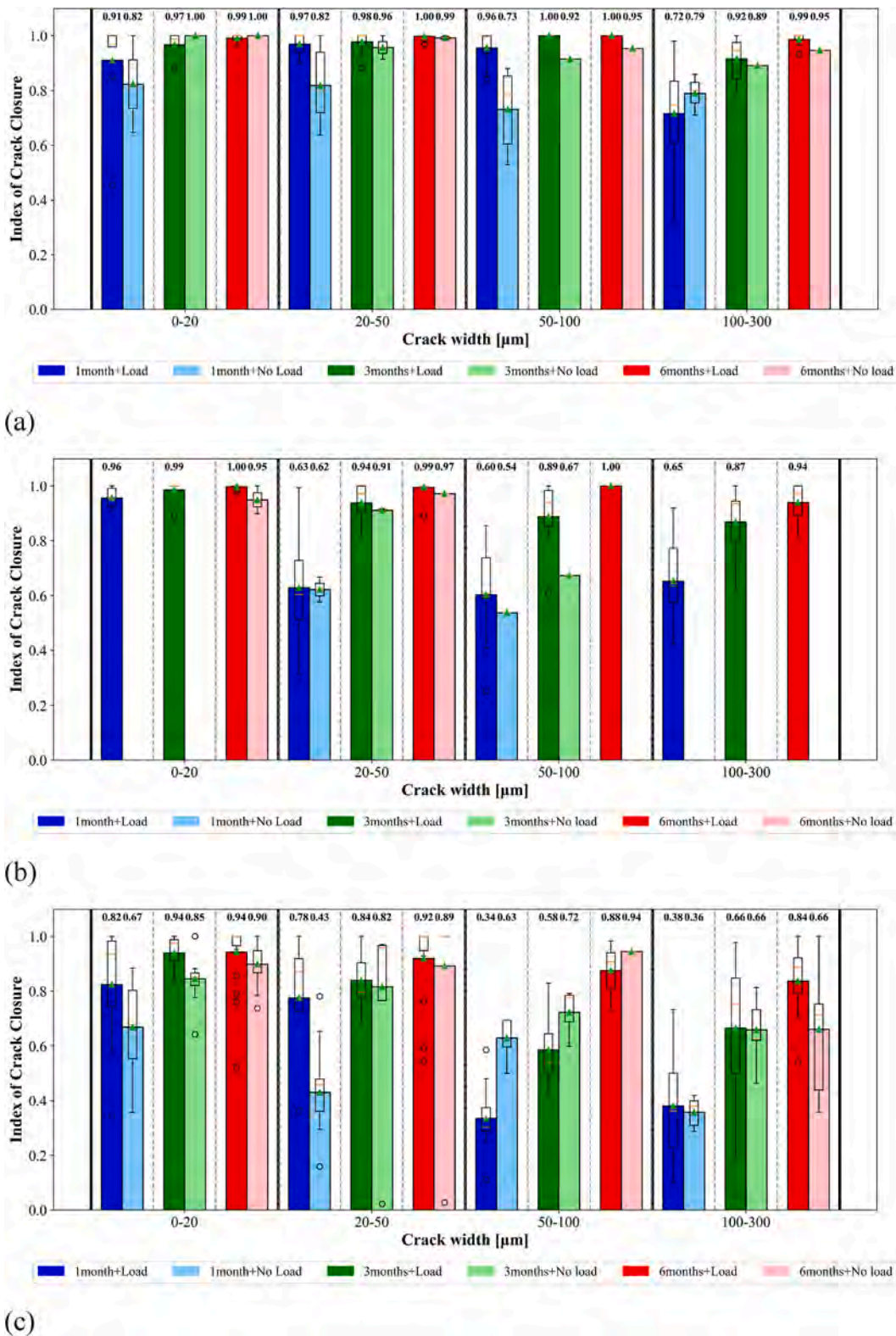
(a)

(b)

(c)

Fig. 10. Effect of sustained load on ICC in different environments (a)tap water; (b)salt water; (c)geothermal water.
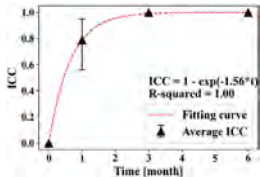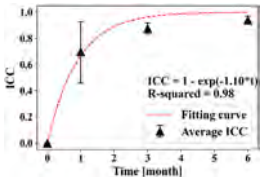
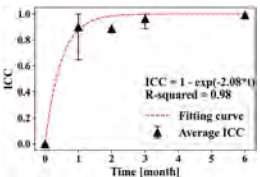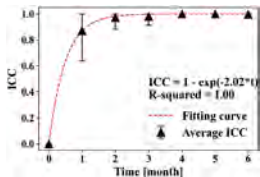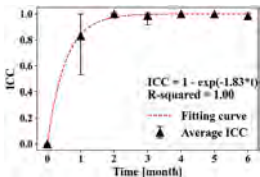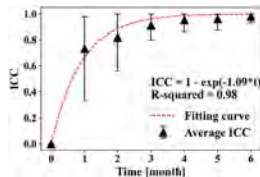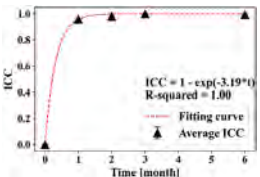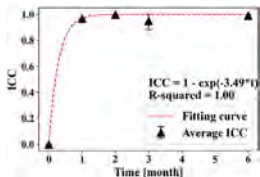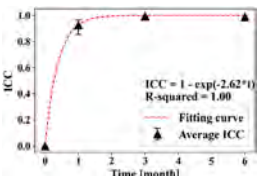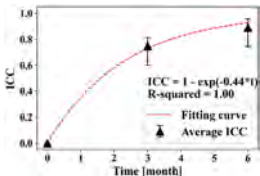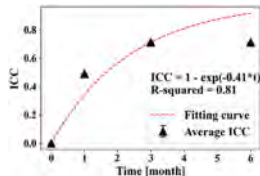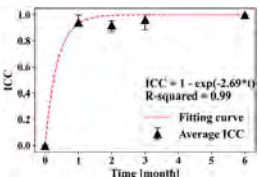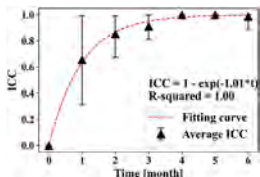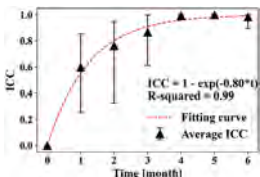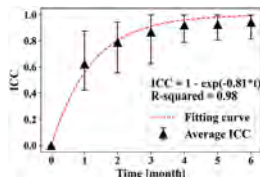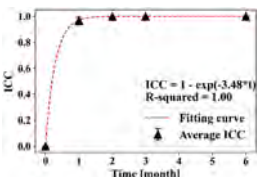environments, mixture designs, and initial crack width. These three main elements significantly influence the kinetics of crack closure crack closure. It is important to acknowledge that, although a substantial number of cracks were collected during the tests, the coefficient S was not obtained for all conditions due to variations in the designs of individual tests. Furthermore, it is pertinent to note that the calibration work on crack self-healing kinetics was restricted to cracks exposed to

aqueous environments. Higher values of S indicate a faster rate of crack closure at a given scale within a predetermined healing environment.
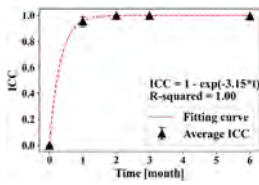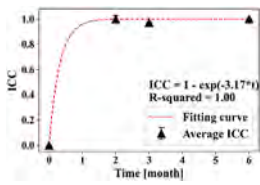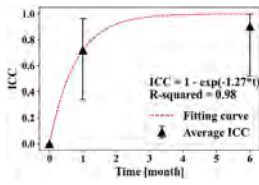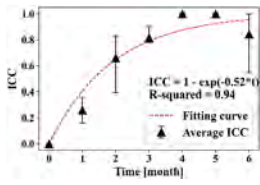
4.2.5. Water exposure environments
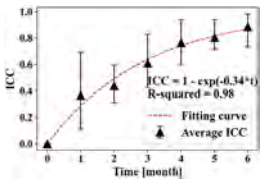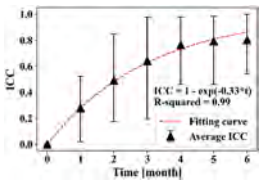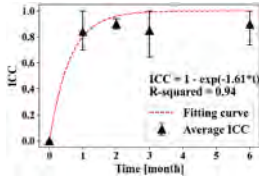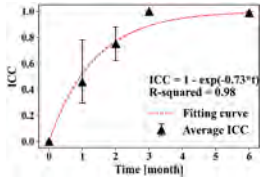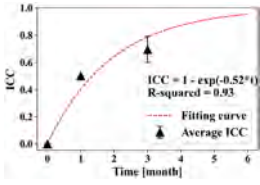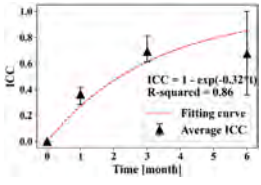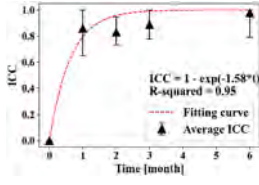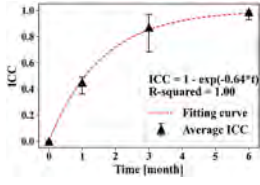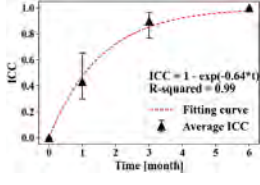
The impact of water environment type on the rate of crack self-healing is highly significant. As illustrated in Fig. 11 the self-healing kinetics coefficient (S) for UHPC with solely CA addition varies across

Table 7
Calibration processes for crack self-healing kinetic coefficient.

Environment	Mix design	Crack width			
		0–20 μm	20–50 μm	50–100 μm	100–300 μm
Tap water	CEM I	–	ICC = 1 − exp(−1.56*t), R-squared = 1.00 S = 1.56 R² = 1.00	ICC = 1 − exp(−1.10*t), R-squared = 0.98 S = 1.10 R² = 0.98	–
	CEM I + CA	ICC = 1 − exp(−2.08*t), R-squared = 0.98 S = 2.08 R² = 0.98	ICC = 1 − exp(−2.02*t), R-squared = 1.00 S = 2.02 R² = 1.00	ICC = 1 − exp(−1.83*t), R-squared = 1.00 S = 1.83 R² = 1.00	ICC = 1 − exp(−1.09*t), R-squared = 0.98 S = 1.09 R² = 0.98
	CEM I + CA + ANF	ICC = 1 − exp(−3.19*t), R-squared = 1.00 S = 3.19 R² = 1.00	ICC = 1 − exp(−3.49*t), R-squared = 1.00 S = 3.49 R² = 1.00	–	–
	CEM I + CA + CNC	ICC = 1 − exp(−2.62*t), R-squared = 1.00 S = 2.62 R² = 1.00	–	–	–
	CEM I + CA + CNF	–	–	–	–
Salt water	CEM I	–	–	ICC = 1 − exp(−0.44*t), R-squared = 1.00 S = 0.44 R² = 1.00	ICC = 1 − exp(−0.41*t), R-squared = 0.81 S = 0.41 R² = 0.81
	CEM I + CA	ICC = 1 − exp(−2.69*t), R-squared = 0.99 S = 2.69 R² = 0.99	ICC = 1 − exp(−1.01*t), R-squared = 1.00 S = 1.01 R² = 1.00	ICC = 1 − exp(−0.80*t), R-squared = 0.99 S = 0.80 R² = 0.99	ICC = 1 − exp(−0.81*t), R-squared = 0.98 S = 0.81 R² = 0.98
	CEM I + CA + ANF	ICC = 1 − exp(−3.48*t), R-squared = 1.00 S = 3.48 R² = 1.00	–	–	–

Table 7 (*continued*)

Environment	Mix design	Crack width			
		0–20 μm	20–50 μm	50–100 μm	100–300 μm
Geothermal water	CEM I + CA + CNC	ICC = 1 - exp(-3.15*t) R-squared = 1.00 S = 3.15 R² = 1.00	ICC = 1 - exp(-3.17*t) R-squared = 1.00 S = 3.17 R² = 1.00	–	–
	CEM I + CA + CNF	–	–	–	–
	CEM I	–	–	–	–
	CEM I + CA	ICC = 1 - exp(-1.27*t) R-squared = 0.98 S = 1.27 R² = 0.98	ICC = 1 - exp(-0.52*t) R-squared = 0.94 S = 0.52 R² = 0.94	ICC = 1 - exp(-0.34*t) R-squared = 0.98 S = 0.34 R² = 0.98	ICC = 1 - exp(-0.33*t) R-squared = 0.99 S = 0.33 R² = 0.99
	CEM I + CA + ANF	ICC = 1 - exp(-1.61*t) R-squared = 0.94 S = 1.61 R² = 0.94	ICC = 1 - exp(-0.73*t) R-squared = 0.98 S = 0.73 R² = 0.98	ICC = 1 - exp(-0.52*t) R-squared = 0.93 S = 0.52 R² = 0.93	ICC = 1 - exp(-0.32*t) R-squared = 0.86 S = 0.32 R² = 0.86
	CEM I + CA + CNC	ICC = 1 - exp(-1.58*t) R-squared = 0.95 S = 1.58 R² = 0.95	ICC = 1 - exp(-0.64*t) R-squared = 1.00 S = 0.64 R² = 1.00	–	–
	CEM I + CA + CNF	–	ICC = 1 - exp(-0.64*t) R-squared = 0.99 S = 0.64 R² = 0.99	–	–

different width scales when exposed to three distinct water environments. Notably, the tap water environment exhibits a higher crack closure rate compared to the other two aggressive environments. This disparity can be attributed to the complex chemical composition of geothermal water, which renders it less efficient in promoting crack healing. Additionally, the chloride component present in salt water also plays a role in the crack healing process.

Further discussion is warranted on the self-healing coefficients in different aqueous environments concerning various crack width ranges. A notable and significant finding emerges in the context of the salt water, where cracks within the width range of 0–20 μm exhibit the most rapid closure rate (S = 2.69). This finding aligns with the results depicted in Fig. 8(a), wherein cracks exposed to salt water for one month showcase high ICC values, ranging from 0.9 to 1, with a consistent density distribution. Comparatively, cracks exposed to tap water in all width ranges possess the highest S-values, indicating that the healing reaction in 0–20 μm cracks, capable of producing $CaCO_3$ in the salt water, is either accelerated or affected by other compound formations covering the cracks.

Similar instances of rapid healing have been observed in other studies. For instance, (Xue et al., 2021) reported that CA-added concrete subjected to repeated wet and dry cycles (40 days) displayed a closure rate of nearly 100% in a chloride ion solution with a concentration of 0.545 mol/L, whereas only about 40% closure was achieved in distilled water. When the chloride ion concentration was increased to 2 mol/L, cracks with an initial width of 50 μm were completely closed within a shorter self-healing period of 30 days. The phenomenon was attributed to Cl^- solution consuming monosulfate (AFm) to form Friedel's salt (Fs), which subsequently decomposes into $Al(OH)_3$ (AH_3) due to carbonation. Throughout this multiphase transformation process, hydroxides are released into the cracking solution, leading to increased dissolved carbon dioxide concentration. Consequently, carbonation of crystals in the cracks accelerates, resulting in rapid crack sealing. However, it is important to note that Friedel salts do not exclusively exert a positive effect on concrete self-healing; numerous tests have demonstrated their detrimental impact on the mechanical properties of concrete (Qiao et al., 2018).

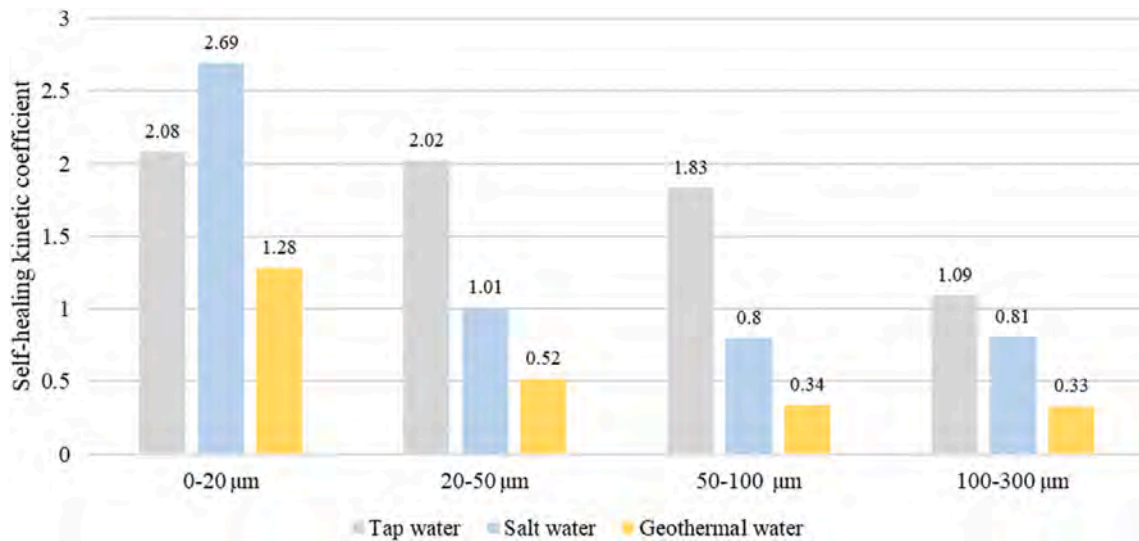In smaller-sized cracks, the presence of chloride ions appears to

Fig. 11. Crack self-healing kinetic coefficients with mix design of CEM I + CA under three water environments.

promote crack closure, but the width threshold for high-rate healing varies due to differences in ion concentration, exposure patterns, and mix design. However, the rate of crack healing decreases significantly when the crack width exceeds approximately 20 μm, as evidenced by the self-healing kinetic coefficient, which decreases and tends to stabilize around 0.8 in the range of crack widths from 20 μm to 300 μm (Fig. 11). Numerous scientific studies consistently demonstrate the detrimental effect of chloride on crack self-healing. It is widely accepted that the main component of the crystalline compounds formed during the healing process is $CaCO_3$, and the presence of chloride hinders the crystallization process and reduces the thermodynamic and kinetic potential of $CaCO_3$ (Borg et al., 2018; Cappellesso et al., 2023). Additionally, chloride infiltration and permeation in cracks are closely related to the crack width. (Maes et al., 2016) proposed a critical crack width of 10 μm, suggesting that cementitious materials with widths below this critical value exhibit no chloride permeation along the crack path. Ismail et al. (2008) conducted chloride diffusion tests and found that cracks up to 30 μm in width had no significant effect on chloride diffusion. However, in a study by Djerbi et al. (2008), the chloride diffusion coefficient increased with increasing crack width within the range of 30 μm–80 μm. Once the crack width exceeded 80 μm, the diffusion coefficient reached a constant value, indicating that it was no longer influenced by material parameters. This observation supports the notion that chloride intrusion is limited when the crack width remains below a specific threshold (20 μm). Beyond this threshold, chloride intrusion into cracks acts as an inhibitor, impeding the crystallization reaction of $CaCO_3$.

The kinetics of crack sealing slowed significantly with increasing crack width, Among the three aqueous environments considered, tap water consistently demonstrated the most favorable conditions for effective crack sealing. Particularly, the reduction in the kinetic coefficient between crack widths of 20 μm, 50 μm, and 100 μm was relatively gradual in this exposure scenario. However, within salt water, a substantial decrease in the kinetic coefficient of self-healing was observed between the 20 μm and 50 μm crack width range, followed by a relatively minor decrease that nearly plateaued beyond 50 μm. Similarly, in geothermal water, there was a sharp reduction in the kinetic coefficient from 20 μm to 50 μm, succeeded by a milder decline. This model suggests that there is a critical threshold between 20 μm and 50 μm below which ionic activity is limited and self-healing can proceed properly. Above this threshold, a delicate equilibrium holds between the leaching or detrimental influence of aggressive ions and the self-healing of cracks.

4.2.6. CA and nanomaterials

Crystalline admixtures (CA) exhibited a positive impact on the self-healing capacity of concrete across various environmental conditions. For instance, in the case of 50–100 μm cracks exposed to tap water, the self-healing coefficient (S) reached approximately 0.7 after the addition of CA in the mixture design. Within this environment, the kinetic coefficient for cracks in the 20–50 μm range increased by less than 0.5 (Fig. 12(a)). This observation suggests the presence of a potential threshold crack width (>50 μm) at which CA is most effective in promoting crystal generation as part of the self-healing process. In salt
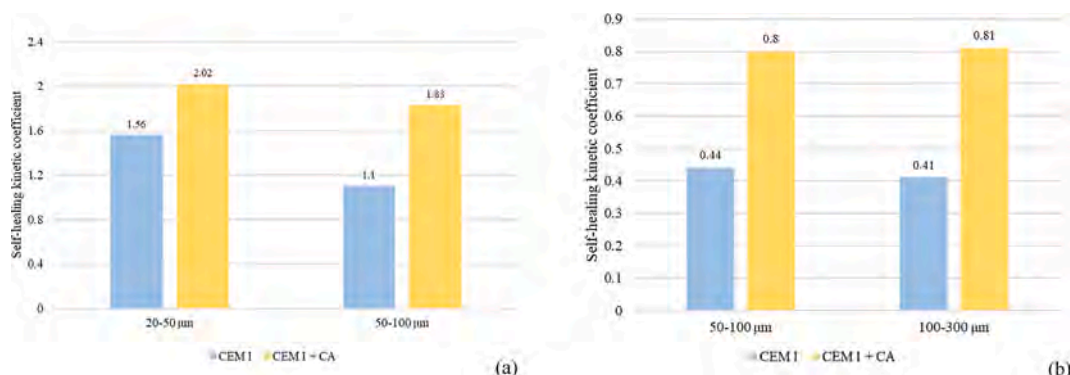

Fig. 12. The effect of CA on crack self-healing kinetic coefficients in (a)tap water; (b) salt water.
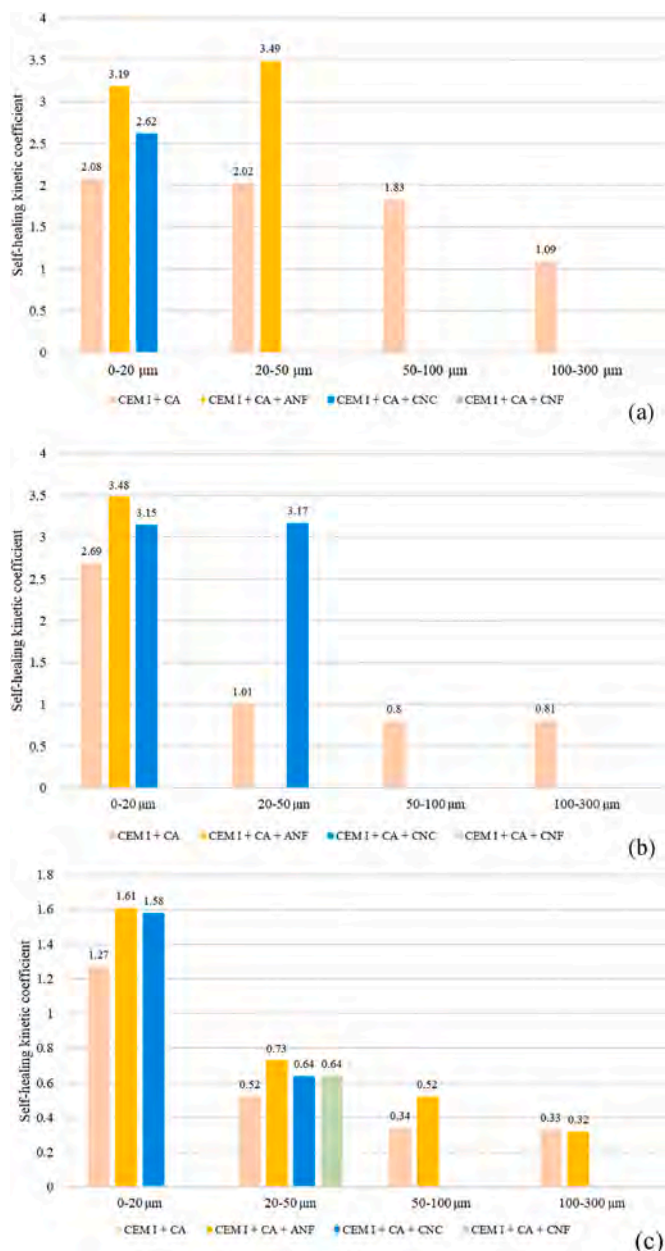
Fig. 13. The effect of nanomaterials on crack self-healing kinetic coefficients in (a) tap water; (b) salt water; (c) geothermal water.

water (Fig. 12(b)), the self-healing coefficients for crack widths of 50–100 μm and 100–300 μm remained constant, with only marginal improvements observed after the addition of CA. This finding further underscores the notion that while CA enhances the rate of crack closure, crack width remains the predominant factor influencing ion intrusion. In fact, CA significantly contributes to the autogenous healing of concrete due to its distinctive reactive silica, specific active substances, and exceptional hydrophilicity, enabling rapid reactions in aqueous environments to participate in crack-sealing processes. The irregular shape of CA in the microscopic and cement-like particles, ranging in size from 0 to 20 μm (Lin et al., 2023), facilitates exploiting the filling benefits of autogenous healing in narrower cracks.

The enhancement of crack healing rate by the addition of nanomaterials depends on both the exposure environment and the crack width. In tap water, the cracks healed very well without the addition of

nanomaterials, while the addition of ANF and CNC had a dramatic change in S, which increased in the range of 0.6–1.1 for cracks of 0–20 μm (Fig. 13(a)). In salt water, cracks at this scale still maintain the best closure as mentioned above, while the addition of nanomaterials raises the kinetic coefficient to a new level (CEM I + CA + ANF: S = 3.48). A remarkable finding emerged when examining the 20–50 μm crack width range, with CNC preserving the self-healing capacity akin to that observed within the 0–20 μm range (S = 3.17), whereas the CA-only addition of the cracks in the range of 20–50 μm has clearly exceeded the threshold in the salt-water environment as mentioned before, thus reducing the S to 1.01 (Fig. 13(b)). This demonstrates that the presence of CNC significantly reduces the negative effect of chloride ions entering the cracks on the self-healing response. Cracks exposed to extreme aggressive environments with ANF-added concrete had higher S values, although the difference with the healing effect presented by other nanomaterials was small. The nanomaterials have a good closure effect on cracks of 0–20 μm in this environment, and when S exceeds 1.6, the ICC can exceed 0.8 after a month. The effect of ANF in stimulating CA work and accelerating calcium carbonate crystal generation decreases with increasing width, and the contribution of the presence of ANF to the healing of cracks tends to zero when the crack exceeds 100 μm (Fig. 13(c)).

The incorporation of CA and nanomaterials during the mix design phase is aimed on the one hand at contributing to the high efficiency of the crack width control capacity (Cuenca et al., 2021a) and, on the other, at expediting crack closure within the healable width by activating the autogenous healing capacity of the concrete. This intervention halts the continuous infiltration of corrosive ions through the cracks, preventing the full penetration of the corrosion phenomenon into the UHPC matrix even under sustained loading and through crack tensile stress (Davolio et al., 2023; Xi et al., 2024). In this self-healing mode, mechanical properties can be harnessed to a certain extent, relying on the efficiency of rapid crack closure. Microscopic studies conducted at the crack interface revealed that the healing products in self-healing lack an adhering effect (Xue et al., 2020). Consequently, In comparison to concrete repaired through autonomous healing principles, the role of CA and nanomaterials in enhancing mechanical properties is confined to the protective stage, ensuring effective crack closure but yielding limited improvement in mechanical characteristics.

5. Indications of threshold crack width

Fig. 14 provides an overview of the crack width ranges, as presented in Tables 5 and 6, necessary to achieve specified ICC values (0.6, 0.8, 1) in various water environments. To establish a definitive healable threshold width, the theoretical time required to attain the specified ICC was computed in conjunction with the kinetic models, resulting in a comprehensive qualitative analysis (Table 8). In the case of tap water, cracks ranging between 50 and 100 μm exhibit complete closure after one month of exposure, with all ICC values reaching 0.8 across size ranges. Utilizing the kinetic analysis, it was determined that cracks within 100 μm attain 80% area closure in less than a month, thus defining 100 μm as the healable threshold width in this environment. Additionally, for salt water, complete closure occurs within the 20–50 μm range after one month, with the ICC reaching 0.8. Linear fitting results suggest 20 μm as the maximum width, a value supported by kinetic assessments demonstrating particularly efficient closure for cracks narrower than 20 μm. Geothermal water also adopts 20 μm as its healable threshold width. Although it is in the 0–20 μm range that cracks with remarkably small widths could be fully healed, considering that the ICC reached 0.6 in less than a month, and in this range, cracks could be partially closed in up to 80% of the area due to the external additives that were used to counteract the effects of this aggressive environment.
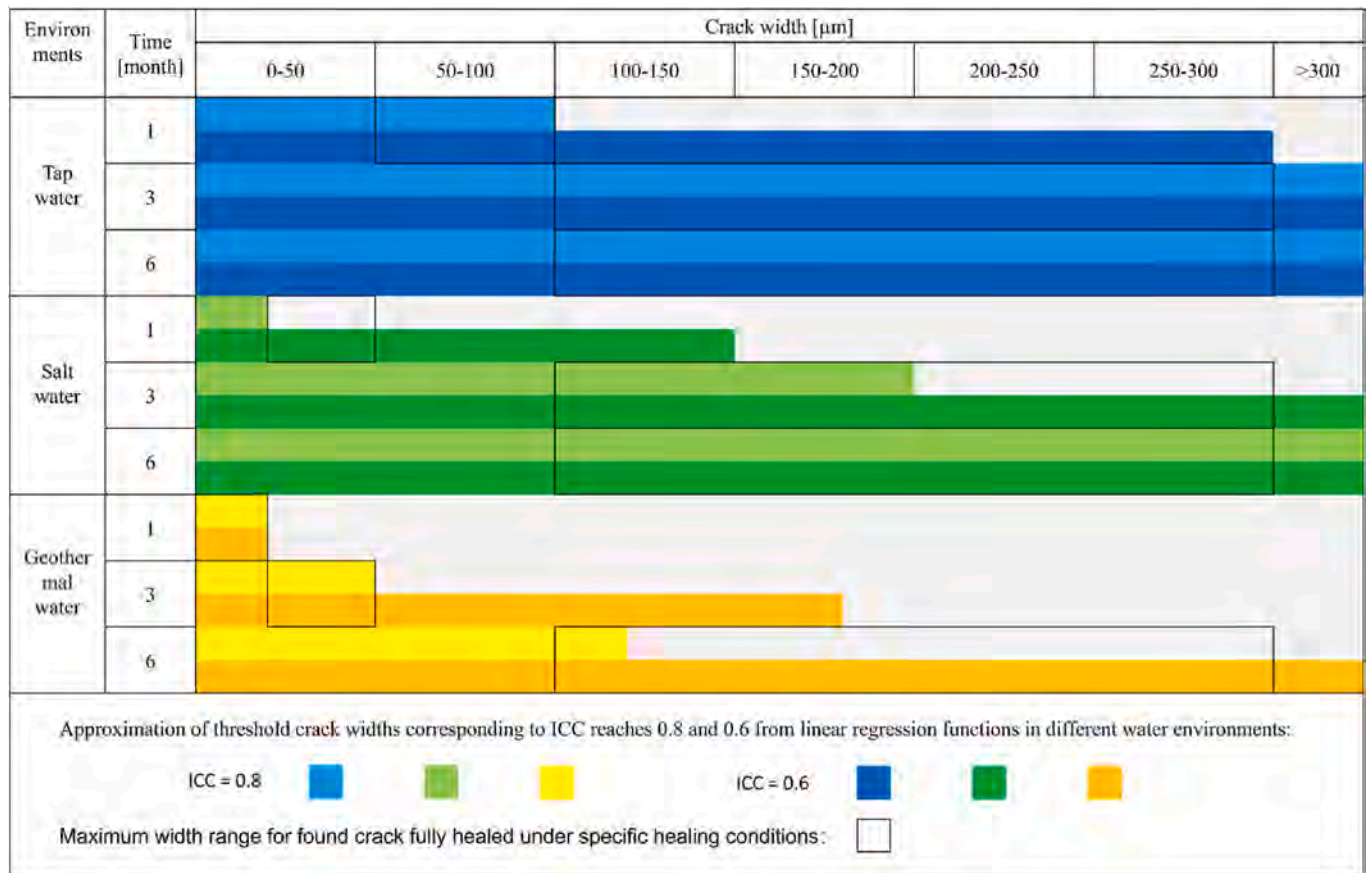
Fig. 14. Summary of threshold width indicators.

Table 8

With mixtures designed as CEM I + CA, the time (Unit: month) required to specify the ICC is deduced from the kinetic modelling.

Required exposure time [month]	0–20 μm		20–50 μm		50–100 μm		100–300 μm	
	ICC		ICC		ICC		ICC	
	0.8	0.6	0.8	0.6	0.8	0.6	0.8	0.6
Tap water	0.8	0.5	0.8	0.5	0.9	0.5	1.5	0.9
Salt water	0.6	0.4	1.6	0.9	2	1.2	2	1.1
Geothermal water	1.3	0.7	3	1.8	4.7	2.7	4.9	2.8

6. Conclusions

The central aim of this research has been to conduct a comprehensive statistical analysis of the crack healing database (more than 700 cracks), which originates from an extensive experimental investigation which has spanned over five years and has been performed in the framework of the Horizon 2020 ReSHEALience project. The study entails defining healable crack width thresholds for specific conditions and calibrating the kinetic law of crack self-healing in ultra-high strength concrete for various aqueous environments. Furthermore, the effects have been analyzed of mixture design, exposure environment, exposure duration, and sustained loading on the evolutionary pattern of crack healing. The principal outcomes of this study can be summarized as follows.

1. Adequate water immersion is conducive to the development of self-healing crystals within cracks, promoting favorable crack closure. However, in geothermal water environments, the kinetic process of $CaCO_3$ formation might be impeded due to the presence of complex chemical constituents, such as sulfur ions. The size of cracks significantly influences the self-healing effect in salt water. This correlation is attributed to chloride activity being associated with crack width. Smaller cracks tend to demonstrate superior self-healing, whereas larger cracks may hinder the efficiency of the self-healing process.

2. Indeed, there is undeniable evidence that crystalline admixtures (CA) enhance the autogenous healing potential of concrete, but the incorporation of nanomaterials must be thoughtfully evaluated in material design, accounting for the specific environment to which the concrete will be exposed. The synergistic interplay of CA with nanomaterials within an environment containing complex ions has the potential to elevate the self-healing coefficient of cracks within the 0–20 μm range, which is effective in improving the healing performance of cracks after only one month of exposure. Additionally, this synergy improves the closure efficiency of cracks with a maximum width of approximately 100 μm.

3. Regarding the impact of crack closure in concrete, sustained loading yields a favorable influence. Two primary observations emerge: (a) loading exerts a more conspicuous effect during the initial stages of exposure, and (b) cracks characterized by smaller widths exhibit greater responsiveness to loading.

4. The derivation of self-healing coefficients (S) through the calibration of crack self-healing kinetics using fitted equations serves a twofold purpose: quantifying healing performance under diverse environments and crack widths, and establishing a theoretical foundation for crack healing modelling, thereby enhancing the precision of UHPC durability assessment. These coefficients, together with "healable crack width thresholds" for specific conditions, allow for the determination of a conservative critical value that ensures complete crack healing while accounting for concrete deterioration caused by

external substance intrusion. For exposure to tap water, a crack width of 100 μm can be considered as the threshold value, with a corresponding self-healing kinetic coefficient of approximately 2, which implies that within a span of two weeks, the ICC can achieve values surpassing 0.6, and within one month, it can exceed 0.8. In contrast, in other two water environments, the critical value for crack width is reduced to 20 μm, striking a balance between healing rate and prevention of ongoing harmful substance infiltration. In salt, cracks measuring 0–20 μm (approximately S = 3) indicate that within a mere two weeks, nearly 80% of the crack area was filled, and by the end of one month, the cracks were nearly fully closed. In geothermal water, although crack healing in this width range can reach 0.8 after one month of exposure, the presence of complex ions substantially hinders the self-healing ability of the cracks as their width increases.

CRediT authorship contribution statement

Zhewen Huang: Writing – review & editing, Writing – original draft, Visualization, Funding acquisition, Formal analysis, Data curation, Conceptualization. **Estefania Cuenca:** Writing – review & editing, Supervision, Methodology, Investigation, Data curation, Conceptualization. **Liberato Ferrara:** Writing – review & editing, Supervision, Resources, Project administration, Methodology, Funding acquisition, Conceptualization.

Declaration of competing interest

The authors declare that they have no known competing financial interests or personal relationships that could have appeared to influence the work reported in this paper.

Data availability

Data will be made available on request.

Acknowledgements

References

Al-Obaidi, S., Bamonte, P., Luchini, M., Mazzantini, I., Ferrara, L., 2020. Durability-based design of structures made with ultra-high-performance/ultra-high-durability concrete in extremely aggressive scenarios: application to a geothermal water basin case study. Infrastructure 5, 102. https://doi.org/10.3390/infrastructures5110102.

Al-Obaidi, S., Bamonte, P., Animato, F., Lo Monte, F., Mazzantini, I., Luchini, M., Scalari, S., Ferrara, L., 2021. Innovative design concept of Cooling water Tanks/basins in geothermal power plants using ultra-high-performance fiber-reinforced concrete with enhanced durability. Sustainability 13, 9826. https://doi.org/10.3390/su13179826.

Al-Obaidi, S., Davolio, M., Monte, F.L., Costanzi, F., Luchini, M., Bamonte, P., Ferrara, L., 2022. Structural validation of geothermal water basins constructed with durability enhanced ultra high performance fiber reinforced concrete (Ultra High Durability Concrete). Case Stud. Constr. Mater. 17, e01202 https://doi.org/10.1016/j.cscm.2022.e01202.

Anwar, A., Mohammed, B.S., Wahab, M.A., Liew, M.S., 2020. Enhanced properties of cementitious composite tailored with graphene oxide nanomaterial - a review. Developments in the Built Environment 1, 100002. https://doi.org/10.1016/j.dibe.2019.100002.

Borg, R.P., Cuenca, E., Gastaldo Brac, E.M., Ferrara, L., 2018. Crack sealing capacity in chloride-rich environments of mortars containing different cement substitutes and crystalline admixtures. Journal of Sustainable Cement-Based Materials 7, 141–159. https://doi.org/10.1080/21650373.2017.1411297.

Cappellesso, V., Di Summa, D., Pourhaji, P., Prabhu Kannikachalam, N., Dabral, K., Ferrara, L., Cruz Alonso, M., Camacho, E., Gruyaert, E., De Belie, N., 2023. A review of the efficiency of self-healing concrete technologies for durable and sustainable concrete under realistic conditions. Int. Mater. Rev. 68, 556–603. https://doi.org/10.1080/09506608.2022.2145747.

Cuenca, E., Ferrara, L., 2017. Self-healing capacity of fiber reinforced cementitious composites. State of the art and perspectives. KSCE J. Civ. Eng. 21, 2777–2789. https://doi.org/10.1007/s12205-017-0939-5.

Cuenca, E., Tejedor, A., Ferrara, L., 2018. A methodology to assess crack-sealing effectiveness of crystalline admixtures under repeated cracking-healing cycles. Construct. Build. Mater. 179, 619–632. https://doi.org/10.1016/j.conbuildmat.2018.05.261.

Cuenca, Estefania, D'Ambrosio, L., Lizunov, D., Tretjakov, A., Volobujeva, O., Ferrara, L., 2021a. Mechanical properties and self-healing capacity of ultra high performance Fibre reinforced concrete with alumina nano-fibres: tailoring ultra high durability concrete for aggressive exposure scenarios. Cem. Concr. Compos. 118, 103956 https://doi.org/10.1016/j.cemconcomp.2021.103956.

Cuenca, E., Lo Monte, F., Moro, M., Schiona, A., Ferrara, L., 2021c. Effects of Autogenous and Stimulated Self-Healing on Durability and Mechanical Performance of UHPFRC: Validation of Tailored Test Method through Multi-Performance Healing-Induced Recovery Indices. Sustainability 13, 11386. https://doi.org/10.3390/su132011386.

Cuenca, Estefania, Mezzena, A., Ferrara, L., 2021b. Synergy between crystalline admixtures and nano-constituents in enhancing autogenous healing capacity of cementitious composites under cracking and healing cycles in aggressive waters. Construct. Build. Mater. 266, 121447 https://doi.org/10.1016/j.conbuildmat.2020.121447.

Cuenca, E., Criado, M., Gimenez, M., Alonso, M.C., Ferrara, L., 2021d. Durability of ultra-high performance fiber reinforced cementitious composites exposed to chemically aggressive environments: up-grading to ultra-high durability concrete through nano-constituents. ASCE J. Mater. Civ. Eng.

Cuenca, E., Criado, M., Giménez, M., Alonso, M.C., Ferrara, L., 2022. Effects of alumina nanofibers and Cellulose nanocrystals on durability and self-healing capacity of ultrahigh-performance fiber-reinforced concretes. J. Mater. Civ. Eng. 34, 04022154 https://doi.org/10.1061/(ASCE)MT.1943-5533.0004375.

Cuenca, E., Postolachi, V., Ferrara, L., 2023. Cellulose nanofibers to improve the mechanical and durability performance of self-healing Ultra-High Performance Concretes exposed to aggressive waters. Construct. Build. Mater. 374, 130785 https://doi.org/10.1016/j.conbuildmat.2023.130785.

Davolio, M., Al-Obaidi, S., Altomare, M.Y., Lo Monte, F., Ferrara, L., 2023. A methodology to assess the evolution of mechanical performance of UHPC as affected by autogenous healing under sustained loadings and aggressive exposure conditions. Cem. Concr. Compos. 139, 105058 https://doi.org/10.1016/j.cemconcomp.2023.105058.

De Belie, N., Gruyaert, E., Al-Tabbaa, A., Antonaci, P., Baera, C., Bajare, D., Darquennes, A., Davies, R., Ferrara, L., Jefferson, T., Litina, C., Miljevic, B., Otlewska, A., Ranogajec, J., Roig-Flores, M., Paine, K., Lukowski, P., Serna, P., Tulliani, J.-M., Vucetic, S., Wang, J., Jonkers, H.M., 2018. A review of self-healing concrete for damage management of structures. Adv. Mater. Interfac. 5, 1800074 https://doi.org/10.1002/admi.201800074.

De Souza Oliveira, A., Da Fonseca Martins Gomes, O., Ferrara, L., De Moraes Rego Fairbairn, E., Toledo Filho, R.D., 2021. An overview of a twofold effect of crystalline admixtures in cement-based materials: from permeability-reducers to self-healing stimulators. J. Build. Eng. 41, 102400 https://doi.org/10.1016/j.jobe.2021.102400.

Djerbi, A., Bonnet, S., Khelidj, A., Baroghel-Bouny, V., 2008. Influence of traversing crack on chloride diffusion into concrete. Cement Concr. Res. 38, 877–883. https://doi.org/10.1016/j.cemconres.2007.10.007.

Ferrara, L., Krelani, V., Carsana, M., 2014. A "fracture testing" based approach to assess crack healing of concrete with and without crystalline admixtures. Construct. Build. Mater. 68, 535–551. https://doi.org/10.1016/j.conbuildmat.2014.07.008.

Ferrara, L., Krelani, V., Moretti, F., 2016. Autogenous healing on the recovery of mechanical performance of High Performance Fibre Reinforced Cementitious Composites (HPFRCCs): Part 2 – correlation between healing of mechanical performance and crack sealing. Cement Concr. Compos. 73, 299–315. https://doi.org/10.1016/j.cemconcomp.2016.08.003.

Ferrara, L., Krelani, V., Moretti, F., Roig Flores, M., Serna Ros, P., 2017. Effects of autogenous healing on the recovery of mechanical performance of high performance fibre reinforced cementitious composites (HPFRCCs): Part 1. Cement Concr. Compos. 83, 76–100. https://doi.org/10.1016/j.cemconcomp.2017.07.010.

Ferrara, L., Van Mullem, T., Alonso, M.C., Antonaci, P., Borg, R.P., Cuenca, E., Jefferson, A., Ng, P.-L., Peled, A., Roig-Flores, M., Sanchez, M., Schroefl, C., Serna, P., Snoeck, D., Tulliani, J.M., De Belie, N., 2018. Experimental characterization of the self-healing capacity of cement based materials and its effects on the material performance: a state of the art report by COST Action SARCOS WG2. Construct. Build. Mater. 167, 115–142. https://doi.org/10.1016/j.conbuildmat.2018.01.143.

Gupta, S., Al-Obaidi, S., Ferrara, L., 2021. Meta-analysis and machine learning models to optimize the efficiency of self-healing capacity of cementitious. Material. Materials 14, 4437. https://doi.org/10.3390/ma14164437.

Hager, M.D., Greil, P., Leyens, C., Van Der Zwaag, S., Schubert, U.S., 2010. Self-healing materials. Adv. Mater. 22, 5424–5430. https://doi.org/10.1002/adma.201003036.

Han, B., Zhang, L., Zeng, S., Dong, S., Yu, X., Yang, R., Ou, J., 2017. Nano-core effect in nano-engineered cementitious composites. Compos. Appl. Sci. Manuf. 95, 100–109. https://doi.org/10.1016/j.compositesa.2017.01.008.

Ismail, M., Toumi, A., François, R., Gagné, R., 2008. Effect of crack opening on the local diffusion of chloride in cracked mortar samples. Cement Concr. Res. 38, 1106–1111.

Istratov, A.A., Vyvenko, O.F., 1999. Exponential analysis in physical phenomena. Rev. Sci. Instrum. 70, 1233–1257.

Kannikachalam, N.P., Cailleux, E., De Belie, N., Ferrara, L., 2023. Evaluation of the self-healing capacity of concrete with low-cost macro-capsules. In: MATEC Web of Conferences. Matec, pp. 1–6.

Koch, G.H., Brongers, M.P., Thompson, N.G., Virmani, Y.P., Payer, J.H., 2005. Cost of corrosion in the United States. In: Handbook of Environmental Degradation of Materials. Elsevier, pp. 3–24.

Lin, X., Li, W., Castel, A., Kim, T., Huang, Y., Wang, K., 2023. A comprehensive review on self-healing cementitious composites with crystalline admixtures: design, performance and application. Construct. Build. Mater. 409, 134108 https://doi.org/10.1016/j.conbuildmat.2023.134108.

Liu, F., You, Z., Diab, A., Liu, Z., Zhang, C., Guo, S., 2020. External sulfate attack on concrete under combined effects of flexural fatigue loading and drying-wetting cycles. Construct. Build. Mater. 249, 118224.

Liu, Y., Wang, L., Wei, Y., Sun, C., Xu, Y., 2024. Current research status of UHPC creep properties and the corresponding applications–A review. Construct. Build. Mater. 416, 135120.

Lo Monte, F., Ferrara, L., 2020. Tensile behaviour identification in Ultra-High Performance Fibre Reinforced Cementitious Composites: indirect tension tests and back analysis of flexural test results. Mater. Struct. 53, 145. https://doi.org/10.1617/s11527-020-01576-8.

Lo Monte, F., Ferrara, L., 2021. Self-healing characterization of UHPFRCC with crystalline admixture: experimental assessment via multi-test/multi-parameter approach. Construct. Build. Mater. 283, 122579 https://doi.org/10.1016/j.conbuildmat.2021.122579.

Lo Monte, F., Repesa, L., Snoeck, D., Doostkami, H., Roig-Flores, M., Jackson, S.J.P., Alvarez, A.B., Nasner, M., Borg, R.P., Schröfl, C., Giménez, M., Alonso, M.C., Serna, P., De Belie, N., Ferrara, L., 2024. Multi-performance experimental assessment of autogenous and crystalline admixture-stimulated self-healing in UHPFRCCs: validation and reliability analysis through an inter-laboratory study. Cement Concr. Compos. 145, 105315 https://doi.org/10.1016/j.cemconcomp.2023.105315.

Maddalena, R., Taha, H., Gardner, D., 2021. Self-healing potential of supplementary cementitious materials in cement mortars: sorptivity and pore structure. Developments in the Built Environment 6, 100044. https://doi.org/10.1016/j.dibe.2021.100044.

Maes, M., Snoeck, D., De Belie, N., 2016. Chloride penetration in cracked mortar and the influence of autogenous crack healing. Construct. Build. Mater. 115, 114–124. https://doi.org/10.1016/j.conbuildmat.2016.03.180.

Mirshahmohammad, M., Rahmani, H., Maleki-Kakelar, M., Bahari, A., 2022. Effect of sustained service loads on the self-healing and corrosion of bacterial concretes. Construct. Build. Mater. 322, 126423 https://doi.org/10.1016/j.conbuildmat.2022.126423.

Muhammad, N.Z., Shafaghat, A., Keyvanfar, A., Abd Majid, M.Z., Ghoshal, S.K., Mohammadyan Yasouj, S.E., Ganiyu, A.A., Samadi Kouchaksaraei, M., Kamyab, H., Taheri, M.M., Rezazadeh Shirdar, M., McCaffer, R., 2016. Tests and methods of evaluating the self-healing efficiency of concrete: a review. Construct. Build. Mater. 112, 1123–1132. https://doi.org/10.1016/j.conbuildmat.2016.03.017.

Muzenski, S., Flores-Vivian, I., Sobolev, K., 2019. Ultra-high strength cement-based composites designed with aluminum oxide nano-fibers. Construct. Build. Mater. 220, 177–186.

Nilimaa, J., 2023. Smart materials and technologies for sustainable concrete construction. Developments in the Built Environment 15, 100177. https://doi.org/10.1016/j.dibe.2023.100177.

Peng, J., Hu, S., Zhang, J., Cai, C.S., Li, L., 2019. Influence of cracks on chloride diffusivity in concrete: a five-phase mesoscale model approach. Construct. Build. Mater. 197, 587–596. https://doi.org/10.1016/j.conbuildmat.2018.11.208.

Qian, M., Zuo, Y., Chen, Z., Yin, X., Liu, Y., Yang, W., Chen, Y., 2019. Crystallization of CaCO3 in aqueous solutions with extremely high concentrations of NaCl. Crystals 9, 647. https://doi.org/10.3390/cryst9120647.

Qiao, C., Suraneni, P., Weiss, J., 2018. Damage in cement pastes exposed to NaCl solutions. Construct. Build. Mater. 171, 120–127. https://doi.org/10.1016/j.conbuildmat.2018.03.123.

Qiu, J., Tan, H.S., Yang, E.-H., 2016. Coupled effects of crack width, slag content, and conditioning alkalinity on autogenous healing of engineered cementitious composites. Cement Concr. Compos. 73, 203–212. https://doi.org/10.1016/j.cemconcomp.2016.07.013.

Reinhardt, H.-W., Jooss, M., 2003. Permeability and self-healing of cracked concrete as a function of temperature and crack width. Cement Concr. Res. 33, 981–985. https://doi.org/10.1016/S0008-8846(02)01099-2.

Roig-Flores, M., Moscato, S., Serna, P., Ferrara, L., 2015. Self-healing capability of concrete with crystalline admixtures in different environments. Construct. Build. Mater. 86, 1–11. https://doi.org/10.1016/j.conbuildmat.2015.03.091.

Roig-Flores, M., Pirritano, F., Serna, P., Ferrara, L., 2016. Effect of crystalline admixtures on the self-healing capability of early-age concrete studied by means of permeability and crack closing tests. Construct. Build. Mater. 114, 447–457. https://doi.org/10.1016/j.conbuildmat.2016.03.196.

Rossi, P., Tailhan, J.-L., Le Maou, F., 2013. Comparison of concrete creep in tension and in compression: influence of concrete age at loading and drying conditions. Cement Concr. Res. 51, 78–84.

Sahmaran, M., Yildirim, G., Erdem, T.K., 2013. Self-healing capability of cementitious composites incorporating different supplementary cementitious materials. Cement Concr. Compos. 35, 89–101.

Schröfl, C., Erk, K.A., Siriwatwechakul, W., Wyrzykowski, M., Snoeck, D., 2022. Recent progress in superabsorbent polymers for concrete. Cement Concr. Res. 151, 106648.

Sisomphon, K., Copuroglu, O., Koenders, E.A.B., 2012. Self-healing of surface cracks in mortars with expansive additive and crystalline additive. Cement Concr. Compos. 34, 566–574. https://doi.org/10.1016/j.cemconcomp.2012.01.005.

Snoeck, D., Van Tittelboom, K., Steuperaert, S., Dubruel, P., De Belie, N., 2014. Self-healing cementitious materials by the combination of microfibres and superabsorbent polymers. J. Intell. Mater. Syst. Struct. 25, 13–24. https://doi.org/10.1177/1045389X12438623.

Snoeck, D., Debo, J., De Belie, N., 2020. Translucent self-healing cementitious materials using glass fibers and superabsorbent polymers. Developments in the Built Environment 3, 100012. https://doi.org/10.1016/j.dibe.2020.100012.

Van Tittelboom, K., De Belie, N., 2013. Self-healing in cementitious materials—a review. Materials 6, 2182–2217. https://doi.org/10.3390/ma6062182.

Van Tittelboom, K., De Belie, N., Van Loo, D., Jacobs, P., 2011. Self-healing efficiency of cementitious materials containing tubular capsules filled with healing agent. Cement Concr. Compos. 33, 497–505.

Wang, J., Ersan, Y.C., Boon, N., De Belie, N., 2016. Application of microorganisms in concrete: a promising sustainable strategy to improve concrete durability. Appl. Microbiol. Biotechnol. 100, 2993–3007.

Wang, Y.-S., Lee, H.-S., Lin, R.-S., Wang, X.-Y., 2022. Effect of silicate-modified calcium oxide-based expansive agent on engineering properties and self-healing of ultra-high-strength concrete. J. Build. Eng. 50, 104230 https://doi.org/10.1016/j.jobe.2022.104230.

Xi, B., Al-Obaidi, S., Ferrara, L., 2023a. Effect of different environments on the self-healing performance of Ultra High-Performance Concrete – a systematic literature review. Construct. Build. Mater. 374, 130946 https://doi.org/10.1016/j.conbuildmat.2023.130946.

Xi, B., Huang, Z., Al-Obaidi, S., Ferrara, L., 2023b. Predicting ultra high-performance concrete self-healing performance using hybrid models based on metaheuristic optimization techniques. Construct. Build. Mater. 381, 131261 https://doi.org/10.1016/j.conbuildmat.2023.131261.

Xi, B., Huang, Z., Al-Obaidi, S., Ferrara, L., 2024. Healing capacity of Ultra High Performance Concrete under sustained through crack tensile stresses and aggressive environments. Cement Concr. Compos. 145, 105355 https://doi.org/10.1016/j.cemconcomp.2023.105355.

Xu, J., Peng, C., Wan, L., Wu, Q., She, W., 2020. Effect of crack self-healing on concrete diffusivity: mesoscale dynamics simulation study. J. Mater. Civ. Eng. 32, 04020149 https://doi.org/10.1061/(ASCE)MT.1943-5533.0003214.

Xue, C., Li, W., Qu, F., Sun, Z., Shah, S.P., 2020. Self-healing efficiency and crack closure of smart cementitious composite with crystalline admixture and structural polyurethane. Construct. Build. Mater. 260, 119955 https://doi.org/10.1016/j.conbuildmat.2020.119955.

Xue, C., Li, W., Luo, Z., Wang, K., Castel, A., 2021. Effect of chloride ingress on self-healing recovery of smart cementitious composite incorporating crystalline admixture and MgO expansive agent. Cement Concr. Res. 139, 106252 https://doi.org/10.1016/j.cemconres.2020.106252.

Xue, C., Tapas, M.J., Sirivivatnanon, V., 2023. Cracking and stimulated autogenous self-healing on the sustainability of cement-based materials: a review. Journal of Sustainable Cement-Based Materials 12, 184–206. https://doi.org/10.1080/21650373.2022.2031334.

Yang, Y., Lepech, M.D., Yang, E.-H., Li, V.C., 2009. Autogenous healing of engineered cementitious composites under wet–dry cycles. Cement Concr. Res. 39, 382–390. https://doi.org/10.1016/j.cemconres.2009.01.013.

Yao, J.J., Chu, S.H., 2023. Durability of sustainable marine sediment concrete. Developments in the Built Environment 13, 100118. https://doi.org/10.1016/j.dibe.2022.100118.

Zhang, W., Zheng, Q., Ashour, A., Han, B., 2020. Self-healing cement concrete composites for resilient infrastructures: a review. Compos. B Eng. 189, 107892 https://doi.org/10.1016/j.compositesb.2020.107892.